Title

Exosomal miRNA 16-5p/29a-3p from pancreatic cancer induce adipose atrophy by inhibiting adipogenesis and promoting lipolysis.

Journal

iScience, 27(7)

Authors

Tien, Sui-Chih
Chang, Chin-Chun
Huang, Ching-Hsuan
et al.

Publication Date

2024-07-19

DOI

10.1016/j.isci.2024.110346

iScience

CellPress
OPEN ACCESS

Article

Exosomal miRNA 16-5p/29a-3p from pancreatic cancer induce adipose atrophy by inhibiting adipogenesis and promoting lipolysis

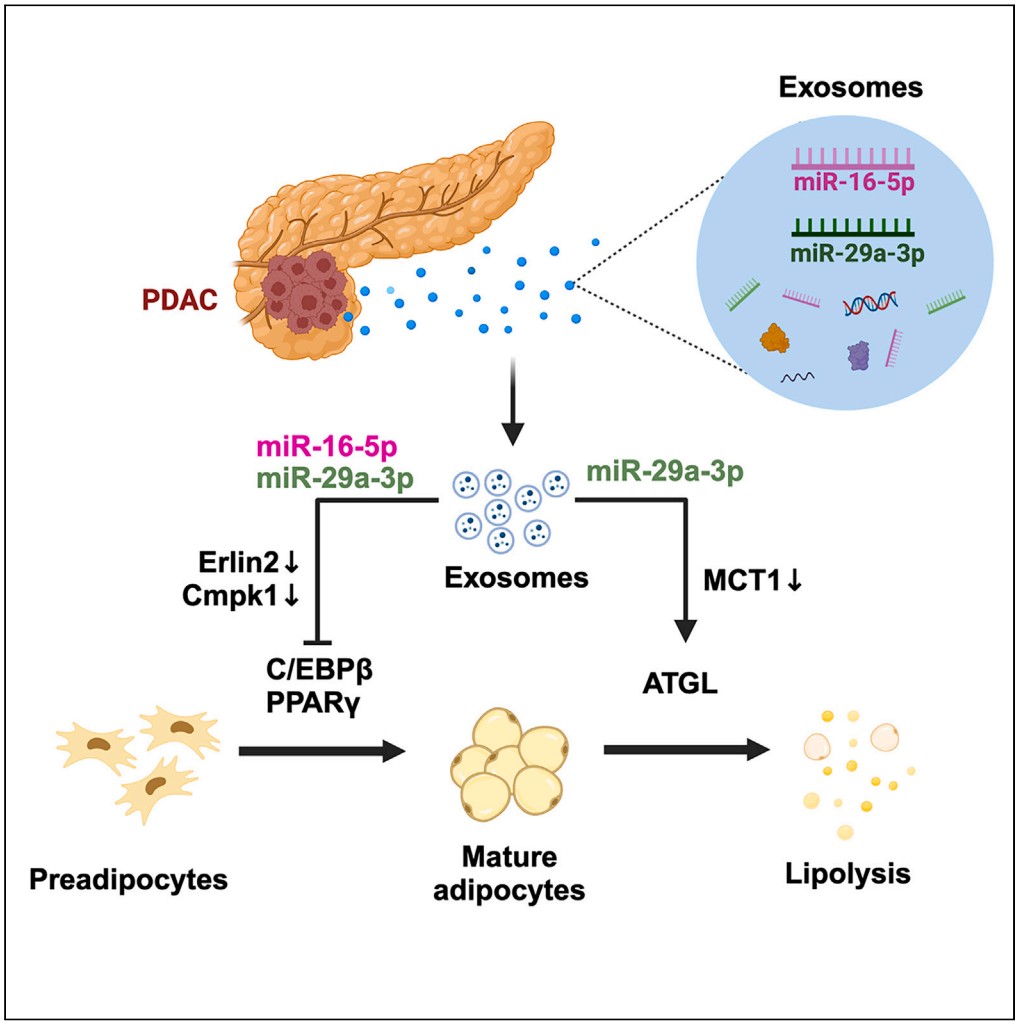

Sui-Chih Tien, Chin-Chun Chang, Ching-Hsuan Huang, ..., Ming-Chu Chang, Wen-Hwa Lee, Chun-Mei Hu

CMHU1220@gate.sinica.edu.tw

Highlights

PDAC-derived exosomes induce fat loss through exosomal miR-16-5p and miR-29a-3p

miR-16-5p and miR-29a-3p impede adipogenesis by targeting Erlin2 and Cmpk1

miR-29a-3p promotes lipolysis via MCT1

Tien et al., iScience 27, 110346
July 19, 2024
https://doi.org/10.1016/j.isci.2024.110346

iScience

CellPress
OPEN ACCESS

Article

Exosomal miRNA 16-5p/29a-3p from pancreatic cancer induce adipose atrophy by inhibiting adipogenesis and promoting lipolysis

Sui-Chih Tien,[1] Chin-Chun Chang,[1] Ching-Hsuan Huang,[1] Hsuan-Yu Peng,[2] Yu-Ting Chang,[2,4] Ming-Chu Chang,[2,3] Wen-Hwa Lee,[1,5,6] and Chun-Mei Hu[1,7,*]

SUMMARY

Over 80% of the patients with pancreatic ductal adenocarcinoma (PDAC) have cachexia/wasting syndrome. Cachexia is associated with reduced survival, decreased quality of life, and higher metastasis rates. Here, we demonstrate that fat loss is the earliest feature of PDAC-exosome-induced cachexia. MicroRNA sequencing of exosomal components from normal and cancer-derived exosomes revealed enrichment of miR-16-5p, miR-21-5p, miR-29a-3p, and miR-125b-5p in serum exosomes of mice harboring PDAC and patients with PDAC. Further, miR-16-5p and miR-29a-3p inhibited adipogenesis through decreasing Erlin2 and Cmpk1 expression which downregulates C/EBPβ and PPARγ. Synergistically, miR-29a-3p promotes lipolysis through increasing ATGL expression by suppressing MCT1 expression. Furthermore, PDAC-exosomes deprived of miR-16-5p and miR-29a-3p fail to induce fat loss. Hence, miR-16-5p and miR-29a-3p exosomal miRs are essential for PDAC-induced fat loss. Thus, we unravel that PDAC induces adipose atrophy via exosomal miRs. This knowledge may provide new diagnostic and therapeutic strategies for PDAC-induced cachexia.

INTRODUCTION

Pancreatic ductal adenocarcinoma (PDAC) is the most aggressive human malignancy which is clinically characterized by local invasion, early metastasis, and resistance to standard chemotherapy.[1] Usually, PDAC is diagnosed late, at unresectable advanced stage[2] and codiagnosed with cachexia.[3] Co-occurrence of cachexia and PDAC is associated with reduced survival, decreased quality of life, and higher rates of metastasis. Interestingly, effective therapeutic interventions of cachexia are expected to significantly improve outcomes for a large proportion of patients with metastatic cancer. However, therapeutics for cachexia remain elusive despite >100 clinical trials targeting its mediators.[3] Worse still, molecular diagnostic options for diagnosing precachexia associated with PDAC are very limited due to the lack of a comprehensive understanding of the underlying disease mechanism. Therefore, elucidating molecular pathophysiology of cachexia co-occurring with PDAC may provide strategies to manage cachexia and increase life quality and reduce mortality in cancer cachexia patients.

Cancer cachexia is a multifactorial metabolic syndrome.[3] Up 80% of late-stage cancer patients suffer from progressive atrophy of adipose tissue and skeletal muscles, resulting in weight loss, treatment resistance, reduced quality of life, and a shortened survival time.[4,5] The prevalence of cancer cachexia, is highest for patients with pancreatic cancer compared to those with other types of cancer.[3]

Fat loss and muscle wasting are striking characteristics of cachexia.[5] Previous studies of pancreatic cancer and cachexia focusing on muscle wasting[6] have shown that various molecules—such as cytokines, hormones, neuropeptides/neurotransmitters, tumor-derived factors, and adipose tissues—activate metabolic pathways which cause skeletal muscle wasting.[6,7] Therapies involving suppression of inflammation (via suppressing cytokines or inhibiting JAK-STAT signaling pathway) and replacing pancreatic enzyme have shown some positive effects in alleviating muscle wasting symptom of cancer cachexia.[8,9] However, the clinical efficacy and safety of these treatments remain to be fully validated.

Unlike studies on skeletal muscle wasting, there is limited understanding of fat loss in cachexia. Most patients suffer from fat loss as cancer progresses. Fat loss in cancer patients is associated with shorter survival but its onset timing and intensity vary among different cancer populations.[10,11] Mounting evidence suggest that cancer cells reprogram the lipid metabolism to meet increasing energy demands and affect cell

[1]Genomics Research Center, Academia Sinica, Taipei 115201, Taiwan
[2]Department of Internal Medicine, National Taiwan University College of Medicine, Taipei 100225, Taiwan
[3]Department of Internal Medicine, National Taiwan University Hospital, Taipei 100225, Taiwan
[4]National Taiwan University Hospital Hsin-Chu Branch, Zhubei City, Hsinchu County 302058, Taiwan
[5]Drug Development Center, China Medical University, Taichung 406040, Taiwan
[6]Department of Biological Chemistry, University of California, Irvine, Irvine, CA 92697, USA
[7]Lead contact
*Correspondence: CMHU1220@gate.sinica.edu.tw
https://doi.org/10.1016/j.isci.2024.110346

proliferation and malignancy.[12] Increased lipolysis may cause fat loss in cancer cachexia,[13–15] however, the precise mechanism of adipose atrophy in cancer cachexia remains elusive.

Exosomes (secreted from various cells and found circulating in the blood) contain a wealth of proteomic and genetic information which can aid in disease diagnostics and disease progress monitoring.[16] Nanoscale exosomes (30–100 nm diameter) are a subtype of heterogeneous population of vesicles secreted by cells which carry DNA, microRNAs (miRNAs), lipids, proteins, and metabolites. They display various biological functions, including inflammatory, immune signaling, coagulatory, vascular reactivity triggering, angiogenic, and tissue repair functions.[17]

Interestingly, extracellular miRNAs act as chemical messengers facilitating cell-cell communication. Free circulating miRNAs associated with proteins such as Ago2[18] or those bound within membrane-bound vesicles, such as exosomes, are more stable.[19,20] Thus, exosomal miRNAs may critically modulate cachexia, including fat loss.

Here, we demonstrated that fat loss is the earliest event in PDAC-induced cachexia. Increases of exosomal miR-16-5p and miR-29a-3p, but not cell-free miRNAs, are identified in the conditional media of PDAC cells and the sera of mice or patients with pancreatic tumors. Treatments with miR-16-5p and miR-29a-3p suppress adipogenesis and enhance lipolysis in adipose tissues of mice. Mechanistically, miR-16-5p and miR-29a-3p inhibit adipogenesis by decreasing the expression of Erlin2 and Cmpk1, leading to downregulation of C/EBPβ and PPARγ, two key transcriptional factors for adipogenesis. Synergistically, miR-29a-3p promotes lipolysis by increasing adipose triglyceride lipase (ATGL) protein expression by suppressing MCT1 expression. Silencing of exosomal miR-16-5p and miR-29a-3p abolishes PDAC-derived exosomes-induced fat loss. These findings demonstrating a key role of exosomal miR-16-5p and miR-29a-3p in adipose atrophy may serve as potential therapeutic targets for pancreatic cancer-mediated cachexia.

RESULTS

Fat loss precedes muscle wasting in PDAC-induced cachexia and it negatively correlates with tumor weight in syngeneic and xenograft mouse models

To investigate PDAC-induced cachexia, we established orthotopic syngeneic mouse models using male C57BL/6J mice and two mouse PDAC (mPDAC) cell lines, Pan18 and KPC. We then analyzed the mouse body composition using NMR, four weeks after orthotopic injection of mPDAC cells into the pancreas of C57BL/6J mice. We found that mice bearing tumors had more fat loss, including body weight loss than the control mice, while their lean mass (muscle mass) remained constant (Figure 1A; Figures S1A and S1B). By gauging the muscle weight, we found that the established mPDAC tumor also affects the weight of quadriceps and triceps (Figure S1C). To affirm whether PDAC-induced fat loss is the first event in cachexia, we measured the body compositions of C57BL/6 mice 2 weeks after inoculation with different numbers of Pan18 cells. We found that body weight and fat mass, but not lean mass, were negatively correlated with the number of the injected Pan18 cells (Figure S1D). These data suggest that fat loss precedes muscle wasting during mPDAC-induced cachexia. Further, mPDAC-induced fat loss was also validated by measuring the weight of adipose tissues (Figures 1B and 1C) (including brown fat (BAT), inguinal fat pads (ingWAT) and gonadal fat pads (gWAT) and adipose size by histological analysis (Figures 1D and 1E). We found that, the fat mass was negatively correlated with tumor weight in these mice (Figure 1F). Further, food and water intakes were similar between the Pan18 inoculated group and the control group (Figure S2A). Therefore, the reduction in fat mass observed in the tumor-bearing mice was not due to a decrease in caloric intake. Additionally, the weights of adipose tissues and quadriceps were significantly lower in Pan18-bearing mice (Figures S2B and S2C).

Since inflammatory status is reportedly associated with cachexia[21,22] and the fat loss could be affected by immune activity, we tested the possibility that the observed fat loss is due to cancer related inflammation. To do this, we created orthotopic xenograft mouse model in immune-deficient male NOD-SCID gamma mice using two human PDAC (hPDAC) patient-derived cell lines—PC080 and PC084—with high metastatic ability.[23] We found that, hPDAC induced fat loss prior to muscle wasting in these immune-deficient mice in a manner similar to that induced by mPDAC in male C57BL/6J mice with normal immune system; hPDAC induced fat loss was positively associated with tumor weight (Figure S3). Taken together, these results suggest that PDAC induces fat loss earlier than muscle wasting, and immune system may not be involved in this process.

PDAC induces fat loss by secreting exosomes

Exosomes signal intercellular communication between the tumor and contiguous organs, highlighting cell-cell communication tools and molecular transfer mechanisms.[24] Silencing of Rab27a and Rab27b, which are critical for multivesicular endosome (MVE) docking at the plasma membrane, significantly inhibits exosome secretion.[25] Thus, to examine the effects of exosomes on PDAC-induced fat loss, we established an mPDAC Pan18 cell line with low exosome secretion capacity by stably expressing Rab27a/b^{shRNA} (via lentivirus infection and puromycin selection). We confirmed that these Rab27a/b knocked down Pan18 cells secreted fewer exosomes than the control cells by using western blot analysis and nanoparticle tracking analysis (NTA) (Figures S4A–S4C). We then injected these cells into the pancreas of mice and found that mPDAC Pan18 cells-induced fat loss and tumor growth were suppressed (Figures S4D–S4F); i.e., stunted exosome secretion via Rab27a/b knockdown impedes tumor growth and fat loss.

Next, to directly demonstrate that PDAC-derived exosomes regulate the PDAC-induced fat loss, we injected near-infrared (NIR) dye DiR-labeled fluorescent exosomes into mice via the orbital injection. To do this, exosomes from culture media of mPDAC (Pan18 and KPC) and normal primary acinar cells were, first, purified and analyzed using ultracentrifugation and NTA (Figures 2A and S5A). Imaging of the injected fluorescent exosomes using *in vivo* imaging system (IVIS) revealed that they target adipose tissues (BAT, gWAT, and ingWAT) (Figure 2B). Interestingly, 4 weeks long treatment with mPDAC-derived exosomes (through daily orbital injection) significantly reduced fat mass and

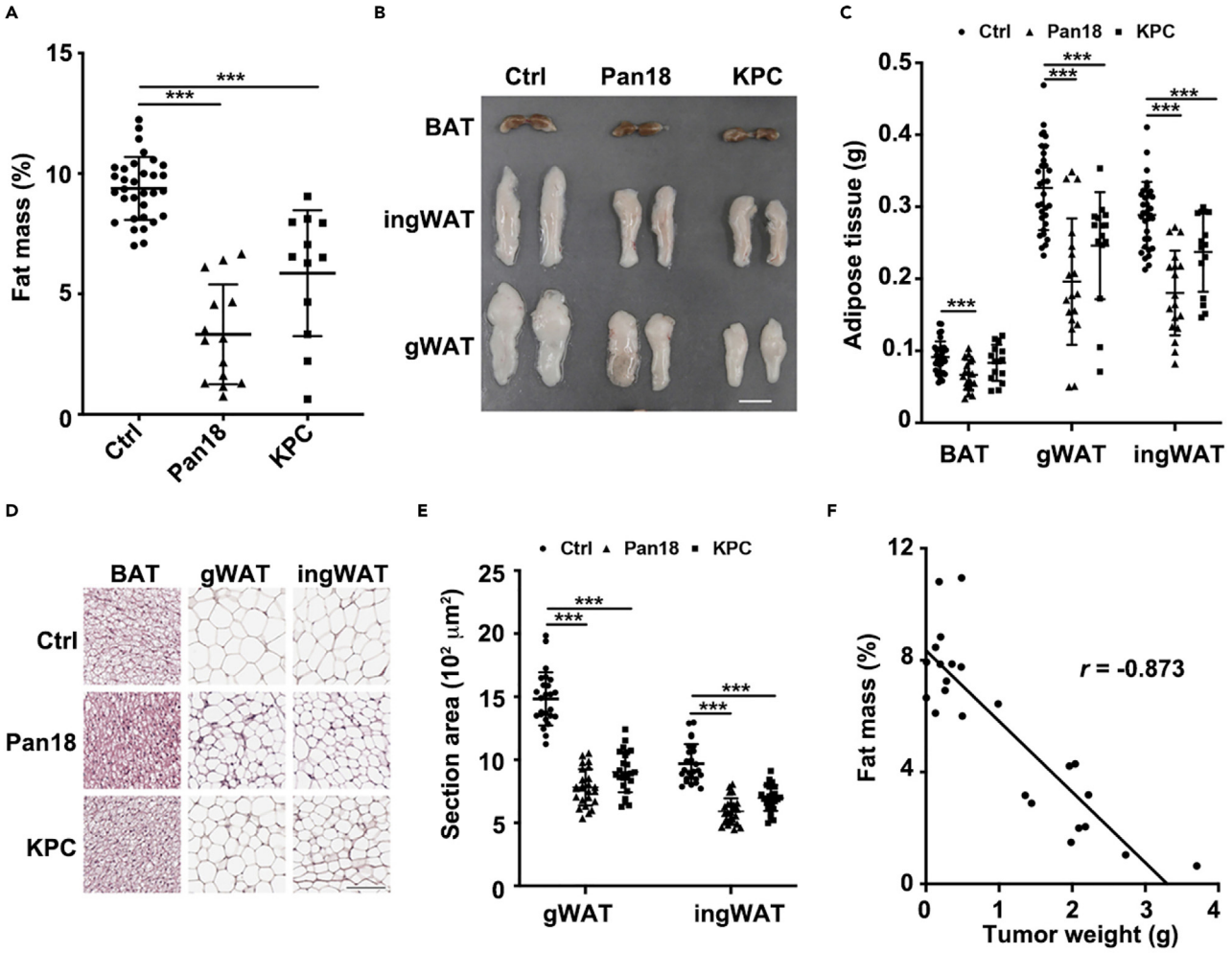

Figure 1. Pancreatic cancer induces adipose atrophy in syngeneic mouse models

C57BL/6 mice inoculated with Pan18 or KPC mouse PDAC cells, (A) Fat mass of control and tumor-inoculated mice measured using NMR (B6 ctrl: $n = 32$; Pan18: $n = 14$; KPC: $n = 12$; data from three independent experiments $N = 3$, one-way ANOVA, $p < 0.0001$).

(B) Representative photograph of brown fat, inguinal fat pads and gonadal fat pads of PDAC cells-inoculated mice (scale bar: 10 mm).

(C) Weight of brown adipose tissue (BAT) and white adipose tissues (WAT) (ctrl: $n = 32$; Pan18: $n = 18$; KPC: $n = 15$; data from three independent experiments; One-way ANOVA, BAT: $p = 0.0019$, gWAT and ingWAT, $p < 0.0001$).

(D) Representative hematoxylin and eosin staining of adipose tissues of control and PDAC-bearing mice (scale bar: 100 µm).

(E) Cross-sectional area of WAT (approximately 2,000–3,000 cells were calculated in five randomly selected views per mice; $n = 5$ mice per group; One-way ANOVA, $p < 0.0001$).

(F) Correlation between fat mass and tumor size in PDAC-bearing mice ([$n = 24$]; values show mean ± SD, *$p < 0.05$, **$p < 0.01$, and ***$p < 0.001$, two-tailed Student's t test).

adipose tissue weight in C57BL6J mice (Figure S5B); whereas treatment with normal acinar cells-derived exosomes did not show these effects (Figures 2C and 2D). These results suggest that PDAC-derived exosomes directly impact adipose atrophy.

PDAC-derived exosomes trigger fat loss by promoting lipolysis and impeding adipogenesis

Next, we deciphered the mechanism of the effect of PDAC-derived exosomes on fat loss. To do so, we first obtained pure exosomes using sucrose gradient purification method[26] (Figure S6A). We ascertained the purity and source of exosomes in the separated fractions using western blotting (with exosomal markers such as Alix, tumor susceptibility gene 101 (TSG101) and CD81) and NTA (Figures S6B–S6F). In addition, the quality of isolated exosomes was validated by electron microscopy (Figure 3A).

To analyze the effects of PDAC-derived exosomes on lipolysis, we treated the differentiated mouse 3T3-L1 cells with these highly purified exosomes (Figure 3B). ATGL is a critical regulator of lipolysis which generates glycerol as the byproduct.[27] Changes in glycerol and ATGL protein levels could reflect the lipolysis condition.[28] We found that the Pan18 cells-derived exosomes increased glycerol (Figure 3C) and

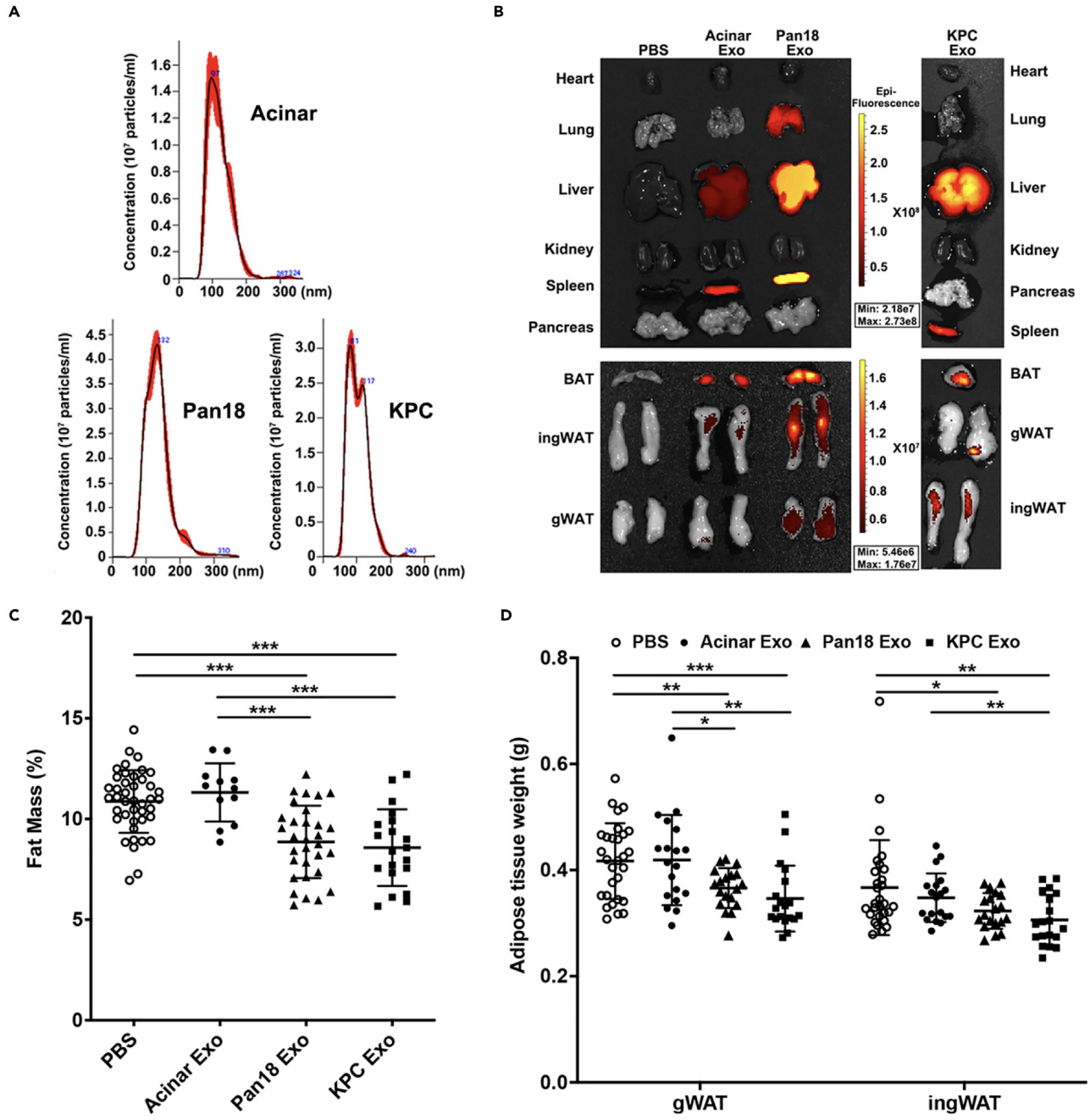

Figure 2. Pancreatic cancer cell-derived exosomes cause adipose atrophy

(A) Nanoparticle tracking analysis (NTA) quantification and size measurement of exosomes isolated from culture medium.

(B) *In vivo* imaging system (IVIS) images of individual organs in C57BL/6 mice postorbital injection of fluorescent DiR-labeled exosomes (50 μg/mice).

(C) Fat mass of C57BL/6 mice, injected daily with/without (w/wo) 10 μg of exosomes, was measured using NMR (PBS: $n = 42$; acinar Exo: $n = 12$; Pan18 Exo: $n = 31$; KPC Exo: $n = 20$; data were from 3 independent experiments ($N = 3$); One-way ANOVA, $p < 0.0001$); The group injected with PBS serves as the control group.

(D) White adipose tissue (WAT) weight in mice treated with exosomes were examined (one-way ANOVA; gWAT: $p = 0.0007$; ingWAT: $p = 0.0079$; PBS: $n = 29$; other group: $n = 19$; data were from 3 independent experiments ($N = 3$), $^{*}p < 0.05$, $^{**}p < 0.01$ and $^{***}p < 0.001$; two-tailed Student's t test).

ATGL levels (Figure 3D) in 3T3-L1 cells in a dose-dependent manner. Further, *in vivo* treatments with Pan18 cells-derived exosomes, elevated the glycerol levels in sera (Figure 3E); and ATGL level was also increased in gWAT and ingWAT adipose tissues (Figure 3F; Figure S6G), whereas normal acinar-derived exosomes did not show these *in vivo* effects. These results suggest that PDAC cells-derived exosomes promote lipolysis by increasing ATGL expression. Since white adipose tissue (WAT) browning (the differentiation of WAT to brown fat) can cause

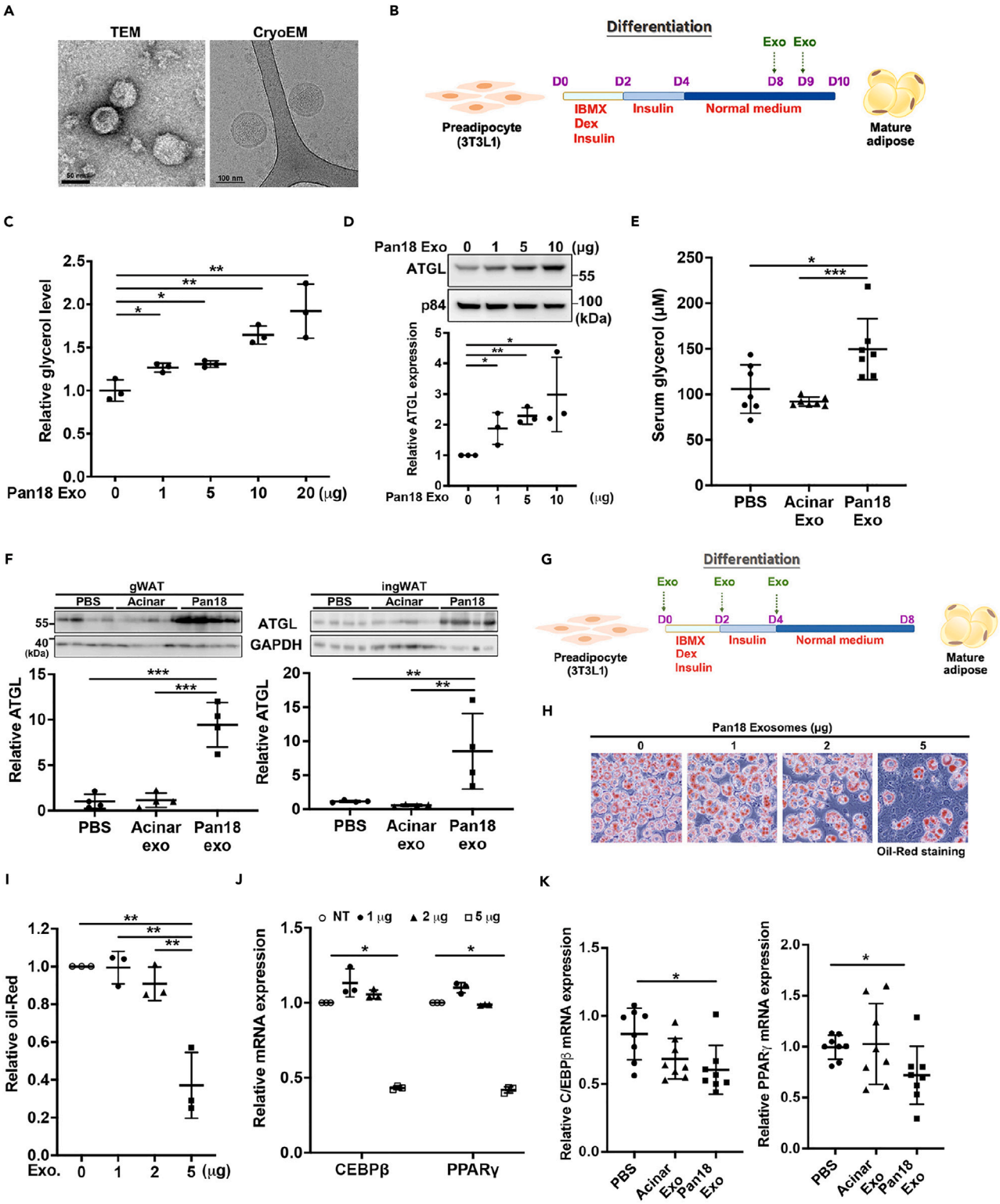

Figure 3. Pancreatic cancer cells-derived exosomes promote lipolysis and impede *in vitro* and *in vivo* adipogenesis

(A) Transmission electron microscopy and cryo-electron microscopy (Cryo-EM) of Pan18 cells-derived exosomes isolated using sucrose gradient.

(B) Schema of the protocol for exosome-induced lipolysis in differentiated mature 3T3-L1 cells.

Figure 3. *Continued*

(C) Mature 3T3-L1 adipocytes were incubated with indicated amounts of purified exosomes for 24 hrs and the concentration of glycerol in the medium was determined. The mean value of Exo-untreated group was normalized to 1.

(D) Western blot analysis of ATGL expression in 3T3-L1 adipocytes treated with various amount of Pan18 exosomes for 24 hrs using ATGL antibody and its quantification (below), (n = 3); p84 was used as internal control.

(E) Glycerol levels were measured in serum from mice injected daily for 4 weeks with PBS, acinar or Pan18 derived exosomes (one-way ANOVA, p = 0.0011).

(F) Western blot analysis of ATGL protein expression in gonadal and inguinal fat pads in exosome-injected C57BL/6 mice. The relative ATGL level is quantified below. p84 was used as internal control and first lane of PBS group was as 1. (values shown as mean ± SD; n = 8; one-way ANOVA; gWAT: $p < 0.0001$, ingWAT: p = 0.0116).

(G) Schema of the protocol for the treatment of differentiating 3T3-L1 cells (preadipocytes) with exosomes.

(H) Cellular lipid contents of exosome-treated 3T3-L1 preadipocytes were assessed using oil-red staining; and (I) stained oil droplets were dissolved and quantified (the oil-red value of untreated 3T3-L1 cells was served as 1 and relative values were shown as mean ± SD; [N = 3]).

(J) mRNA expressions of key adipogenic factors C/EBPβ and PPARγ in 3T3-L1 preadipocytes treated with various exosomes (n = 3).

(K) C/EBPβ and PPARγ mRNA expression in gonadal fat pads from C57BL/6 mice treated with either acinar or Pan18 derived exosomes (The relative levels were quantified and normalized with GAPDH; one mouse from the PBS-injected group was counted as 1. Values show mean ± SD (n = 8); one-way ANOVA, p = 0.0476 and 0.0895; two-tailed Student's t test, $*p < 0.05$, $**p < 0.01$ and $***p < 0.001$).

fat loss mediated by upregulation of uncoupling protein 1 (UCP1) expression,[29] we examined the UCP1 expression in adipose tissues (ingWAT and gWAT) from exosome-injected mice. We found that UCP1 expression levels (measured using qPCR analysis and IHC analysis) were not affected by Pan18 cells-derived exosomes (Figures S7A and S7B). These data indicate that WAT browning may not be involved in the PDAC-exosome-induced fat loss.

Besides lipolysis, impeded adipogenesis is another cause for fat loss. The liposoluble oil red O, a lysochrome diazo dye used for staining neutral triglycerides and lipids, can be used to evaluate the degree of adipocyte differentiation.[30] Additionally, the expressions of peroxisome proliferator-activated receptor γ (PPARγ) and the CCAAT/enhancer-binding (C/EBP) factors, particularly C/EBPβ,[31] which regulate adipogenesis, can also be used to evaluate the degree of adipocyte differentiation.

Here, when differentiating 3T3-L1 cells (preadipocytes) were treated with Pan18 cells-derived exosomes (Figure 3G), oil red O staining (Figures 3H and 3I) and C/EBPβ and PPARγ mRNA levels (Figure 3J) were significantly decreased, suggesting that PDAC-derived exosomes inhibit adipogenesis. To validate this observation *in vivo*, we analyzed the mRNA levels of C/EBPβ and PPARγ in adipose tissues from exosome-injected C57BL/6 mice and found that C/EBPβ and PPARγ mRNAs in gWAT adipose tissues were decreased when injected with Pan18 cells-derived exosomes (Figure 3K). Taken together, these results suggest that PDAC-derived exosomes induce fat loss in two ways: promoting lipolysis and inhibiting adipogenesis.

miR-16-5p/miR-21-5p/miR-29a-3p/miR-125b-5p are highly expressed in the PDAC-derived exosomes

miRNAs are more stable inside membrane-bound vesicles, called exosomes,[20] facilitating their circulation to distant targets. To identify the potential exosomal miRNAs that induce fat loss, we isolated and highly purified the exosomes secreted from normal acinar and PDAC cells as previously described and analyzed their miRNAs composition using small RNA-seq analysis (Data are made available). Briefly, during miRNA expression analysis we removed miRNA with reads <100, and selected miRNA with 2-fold higher expression in PDAC-derived exosomes when compared with that in normal pancreatic cells-derived exosomes (mouse pancreatic acinar cells and human pancreatic ductal HPDE cells) (Figure 4A). This helped us identify 12 miRNAs, which have 2-fold higher expression in at least two PDAC cells (Figure 4B). Next, we used qPCR analysis to validate miRNAs expression levels in these exosomes. We found that four miRNAs—miR-16-5p, miR-21-5p, miR-29a-3p, and miR-125b-5p—had consistently 2-fold higher expression levels in both exosomes derived from mPDAC cells (Pan 18 and KPC) and hPDAC cells than those derived from normal pancreatic cells (Figure S8). To test whether these four miRNAs are upregulated *in vivo*, we analyzed exosomal and cell-free miRNAs in serum (Figure S9) in mice or patients with PDAC. We found that these four miRNAs—miR-16-5p, miR-21-5p, miR-29a-3p, and miR-125b-5p—were expressed highly in exosomes but not in serum (Figures 4C–4J; Figure S10). Thus, these circulate as exosomal miRNAs. These results suggest that these four miRNAs enriched in PDAC-derived exosomes may play roles in PDAC-induced pathogenesis, including fat loss.

miR-16-5p and miR-29a-3p inhibit adipogenesis through reducing Erlin2 and Cmpk1 expression leading to C/EBPβ and PPARγ downregulation

To dissect the roles of the identified four exosomal miRNAs in adipogenesis, we individually transfected them into 3T3-L1 preadipocytes and analyzed their effects on adipogenesis (Figure 5A). Through the oil red staining assay for adipogenesis, we found that all the four candidate miRNAs had an impact on adipogenesis, particularly, miR-16-5p and miR-29a-3p significantly impeded adipogenesis (Figures 5B and 5C). Using western blotting analysis, we found that treatment of 3T3-L1 preadipocytes with miR-16-5p and miR-29a-3p also dramatically downregulated the crucial proteins involved in adipogenesis, namely C/EBPβ and PPARγ (Figure 5D). Furthermore, using the *in vivo*-jetPEI system to directly deliver miRNAs into the inguinal fat pads of mice, we found that individual treatments with miR-16-5p and miR-29a-3p decreased the C/EBPβ and PPARγ protein expression in the adipose tissues (Figures 5E and 5F).

To explore which adipogenesis genes were directly affected by miR-16-5p and miR-29a-3p, we analyzed the target genes predicted using two bioinformatic databases (miRDB and TargetScan), and the 412 proteins pool, which were observed to be downregulated in miR-16-5p

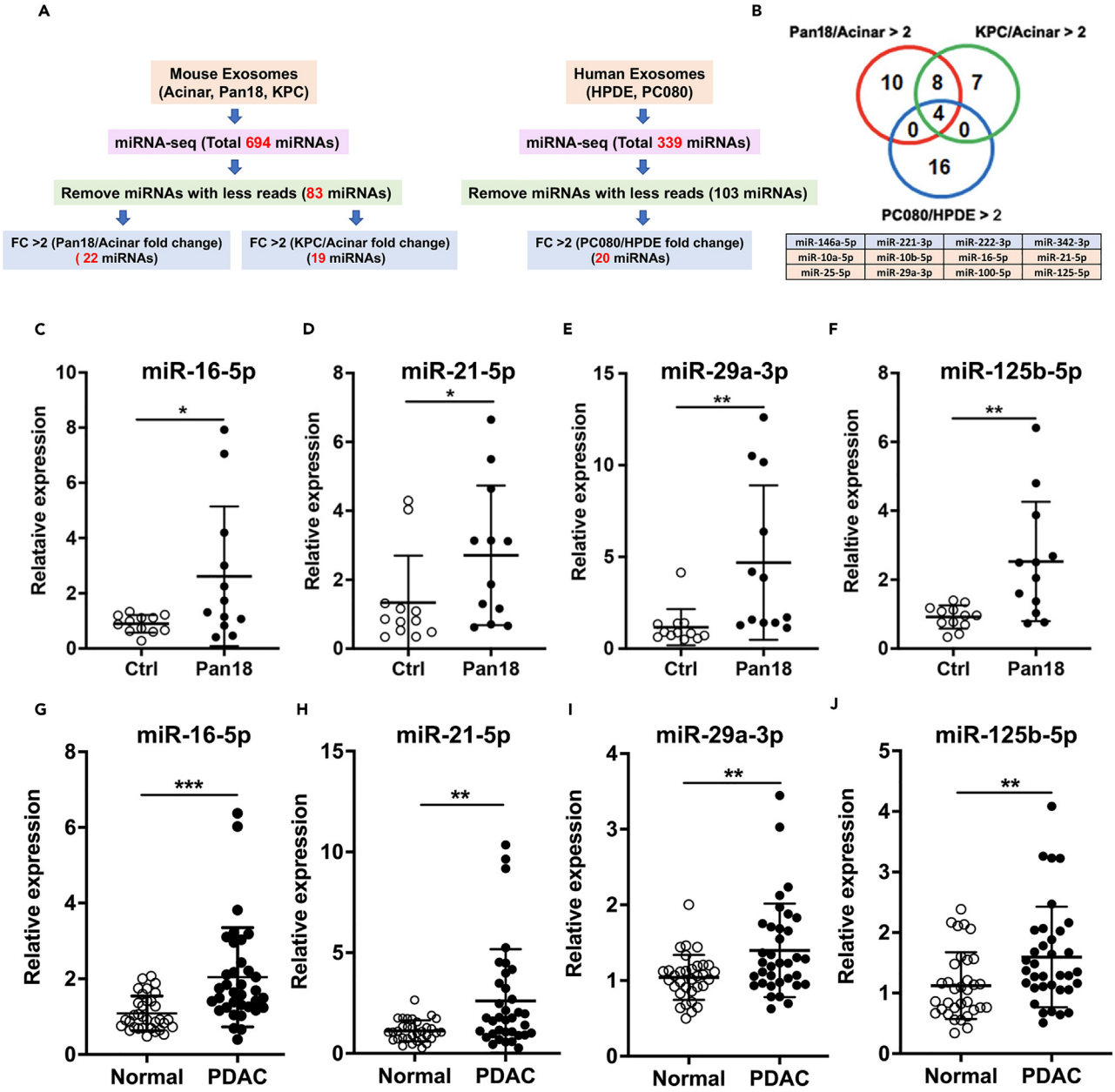

Figure 4. Identification of miRNAs highly expressed in PDAC-derived exosomes

(A) Flowchart depicting the miRNA RNA-seq analysis pipeline.

(B) Venn diagram of miRNAs upregulated in PDAC cells (threshold: log2 fold change >2). The overlap of upregulated miRNAs after injection with Pan18/Acinar (red circle), KPC/Acinar (green circle) and PC080/HPDE (blue circle) are shown in right panels.

(C–F) The candidate miRNA expressions in serum exosomes from tumor-bearing C57BL/6 mice. Ctrl mice were without tumor inoculation. Sno-135 was used as an internal control (n = 12 per group).

(G–J) The candidate miRNA expressions in plasma exosomes from human PDAC patients (RNU44 was used as an internal control; Normal group consists of individuals without PDAC, Normal: n = 33; PDAC: n = 35; Results shown as mean ± SD, two-tailed Student's t test, *$p < 0.05$, **$p < 0.01$ and ***$p < 0.001$).

and miR-29a-3p-transfected 3T3-L1 preadipocytes, using mass spectrometry analysis (Data availability). Using these three datasets, two potential genes, *Erlin 2* (endoplasmic reticulum lipid raft-associated protein 2) and *Cmpk1* (cytidine/uridine monophosphate kinase 1), were identified as direct targets of miR-16-5p and miR-29a-3p (Figure 5G). Erlin2 has been studied as a key ER membrane protein that blocks SREBP activation and regulates cytosolic lipid content.[32] Cmpk1 plays an important role in *de novo* pyrimidine synthesis, which has been reported to have functional relevance during diet-dependent remodeling of adipose tissue.[33] In addition, individual treatments with miR-16-5p

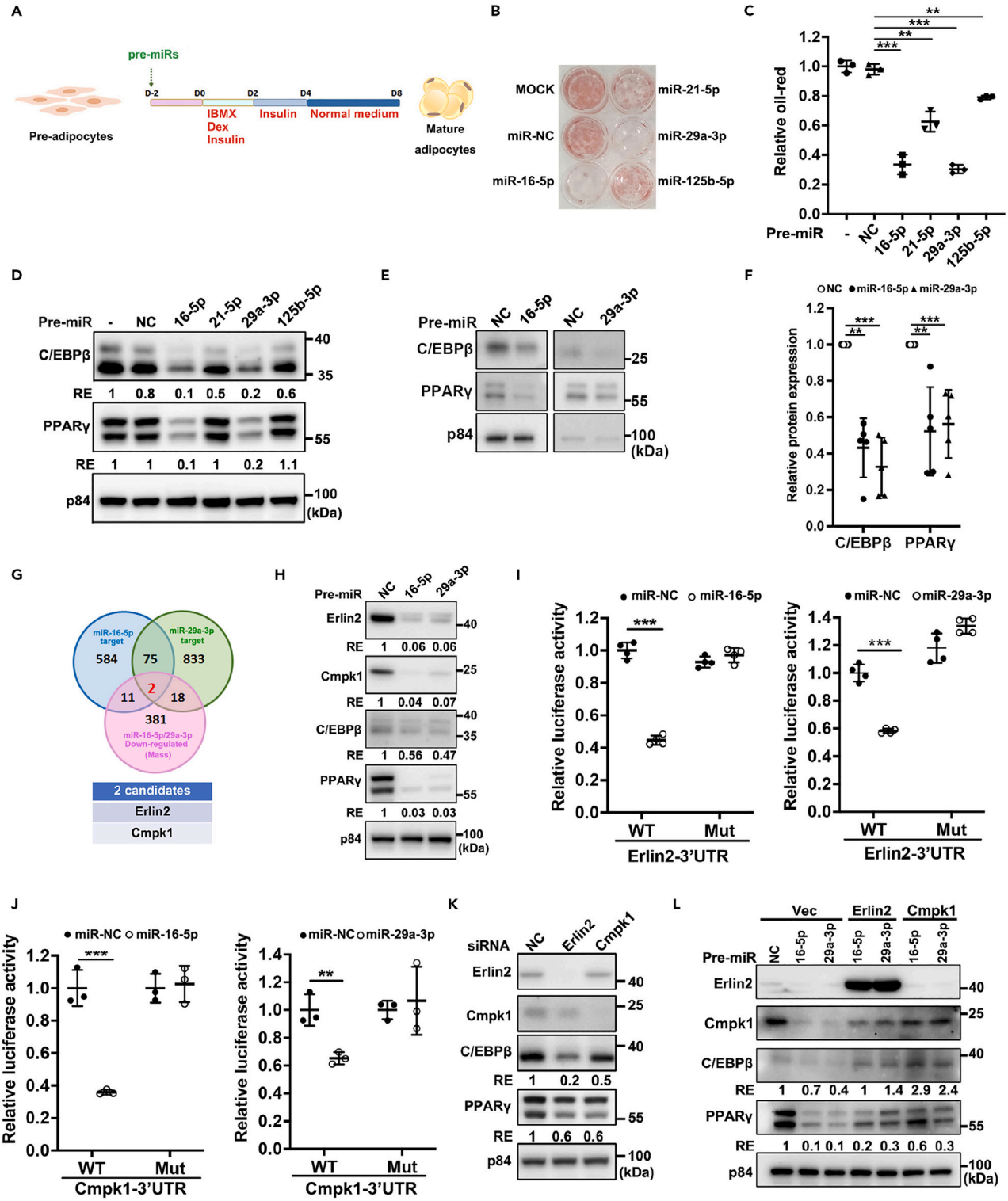

Figure 5. miR-16-5p and miR-29a-3p inhibit adipogenesis by downregulating *Erlin2* and *Cmpk1* expression

(A) Schema of protocol for treatment of 3T3-L1 preadipocytes with pre-miRs.

(B) Oil red O staining of 3T3-L1 preadipocytes treated with 50 nM of miRNAs; MOCK indicates samples without miRNA transfection, while NC represents negative control miRNA.

(C) Quantification of the lipid (Results shown as mean ± SD; *n* = 3).

Figure 5. *Continued*

(D) Western blotting analyses (using C/EBPβ and PPARγ antibodies) of 3T3-L1 preadipocytes transfected with 50 nM of miRNA-mimics for 48 h. The relative expression levels are shown below.

(E) Western blot analyses of C/EBPβ and PPARγ in 4th mammary fat pad from C57BL/6 mice injected with miR-16-5p or miR-29a-3p mimic liposomes for 3 days.

(F) Quantitation of relative C/EBPβ and PPARγ expression in miR-mimic-injected fat pad shown in (E) (n = 5 per group), The value of NC-injected was normalized to 1.

(G) Venn diagram of predicted miR-16-5p and miR-29a-3p target genes (using TargetScan and miRDB database) and miR-downregulated proteins ([Fold change <0.3] revealed using Mass analysis).

(H) Western blot analyses of C/EBPβ, PPARγ, Erlin2, and Cmpk1 in 3T3-L1 cells treated with 50 nM of miR-16-5p or miR-29a-3p.

(I and J) Luciferase activities of the luciferase plasmid constructs containing the wild-type or mutant-type 3′UTR of *Erlin2* (I); and *Cmpk1* (J); upon transfecting with 50 nM miR-16-5p and miR-29a-3p mimics (The relative luciferase activity was measured at 48 h after transfection and normalized to Renilla luciferase activity; Fold change was calculated by the normalized luminescence signal from pre-miR NC as "1." The data are represented as mean ± SD; $^{**}p < 0.01$, $^{***}p < 0.001$ versus control mimics (NC); N = 3); (K) western blot analyses of C/EBPβ and PPARγ in 3T3-L1 adipocytes after knockdown with 25 nM of *Erlin2* or *Cmpk1* siRNA; (L) western blot analyses of C/EBPβ and PPARγ expression in 3T3-L1 cells stably expressing *Erlin2* or *Cmpk1* siRNA after transfection with 50 nM of miR-16-5p or miR-29a-3p mimics (two-tailed Student's t test, $^{**}p < 0.01$ and $^{***}p < 0.001$).

and miR-29a-3p decreased the protein expression levels of Erlin2, Cmpk1, C/EBPβ, and PPARγ in 3T3-L1 preadipocytes (Figure 5H). To address whether *Erlin2* and *Cmpk1* are directly regulated by miR-16-5p and miR-29a-3p, we cloned the 3′UTR regions of these two genes containing the predicted binding sites of miR-16-5p and miR-29a-3p (Figure S11) into the downstream region of a firefly luciferase reporter gene in a pmirGLO vector (*Erlin2*-and *Cmpk1*-luciferase plasmid constructs). We individually cotransfected these *Erlin2*-or *Cmpk1*-luciferase plasmid constructs with miR-16-5p and miR-29a-3p miRNAs into 3T3-L1 preadipocytes. We found that, compared to the negative control miRNA (NC), miR-16-5p and miR-29a-3p significantly reduced the luciferase activity of these *Erlin2*-or *Cmpk1*-luciferase plasmid constructs (Figures 5I and 5J). Meanwhile, miR-16-5p and miR-29a-3p did not affect the luciferase activity of the *Erlin2*-or *Cmpk1*-luciferase plasmid constructs containing the mutated 3′UTR region of *Erlin2* or *Cmpk1* (having low affinity binding to miR-16-5p and miR-29a-3p) (Figures 5I and 5J). These data suggest that *Erlin2* and *Cmpk1* are the direct targets of miR-16-5p and miR-29a-3p.

To further dissect the relationship between *Erlin2*/*Cmpk1*, C/EBPβ and PPARγ, using western blotting, we examined their protein expression levels at various time points during adipogenesis. We found that Erlin2/Cmpk1 were expressed earlier than C/EBPβ and PPARγ (Figure S12). In addition, using siRNA treatment, we found that knockdown of *Erlin2*/*Cmpk1* decreased the expression of C/EBPβ and PPARγ (Figure 5K). Moreover, *Erlin2*/*Cmpk1* overexpression restored miR-16-5p- and miR-29a-3p-induced downregulation of C/EBPβ and PPARγ (Figure 5L). Taken together, these results suggest that miR-16-5p and miR-29a-3p inhibit adipogenesis by targeting *Erlin2* and *Cmpk1* leading to C/EBPβ and PPARγ downregulation.

miR-29a-3p promotes lipolysis by inhibiting MCT-1 expression leading to the ATGL upregulation

Because adipogenesis and lipolysis are involved in fat loss (Figure 3), we also examined the influence of the four highly expressed exosomal miRNAs—miR-16-5p, miR-21-5p, miR-29a-3p, and miR-125b-5p—in lipolysis (Figure 6A). Only miR-29a-3p transfection into the mature 3T3-L1 adipocytes dramatically increased their ATGL levels (Figure 6B). Consistently, the miR-29a-3p transfected mature 3T3-L1 adipocytes releasing significantly higher levels of glycerol (Figure 6C). Using the *in vivo*-jetPEI liposomes system to deliver miR-29a-3p into the inguinal fat pads of mice, we further validated that miR-29a-3p increases ATGL protein levels in adipose tissues (Figure 6D). Thus, miR-29a-3p has a significant role in lipolysis.

To identify the miR-29a-3p direct target involved in increasing ATGL expression, we analyzed the target genes predicted using miRDB and TargetScan databases, and the pool of 60 proteins, which were downregulated in miR-29a-3p-transfected 3T3-L1 cells (data obtained by mass analysis (mass data in Data availability). Two common target genes (monocarboxylate transporter 1 (*MCT1*) and chromosome segregation 1-like (*Csel1*) were identified at the intersection of the predicted genes and downregulated proteins (Figure 6E). Previous study has showed that inhibiting MCT1 has profound effects on adipocyte lipolysis[34] and Cse1l functions as a nuclear transporter for pancreatic cancer proliferation.[35] Using miR-29a-3p transfection, we confirmed that in mature 3T3-L1 adipocytes, miR-29a-3p increases ATGL and dramatically decreases MCT1 expression, but has little effect on Csel1expression (Figure 6F). Thus, MCT1 may be the direct target of miR-29a-3p. To test this, we performed a luciferase reporter assay using a pmirGLO vector encoding the putative miRNA binding site of 3′-UTR of *MCT1* gene (*MCT1*-luciferase construct) (Figure S13). We observed that miR-29a-3p suppressed luciferase activity of the *MCT1*-luciferase construct (Figure 6G). Furthermore, miR-29a-3p failed to suppress the luciferase activity of the *MCT1*-luciferase construct containing the mutated putative miR-29a-3p 3′-UTR binding site of *MCT1* (Figure 6G) Thus, *MCT1* is a direct target of miR-29a-3p.

Further, to test whether *MCT1* expression directly affects ATGL expression, we silenced *MCT-1* using siRNA. We found that ATGL expression levels were increased upon *MCT-1* silencing (Figure 6H), suggesting that MCT1 is a negative regulator of ATGL. Furthermore, to examine whether MCT1 regulates ATGL by direct interaction, we performed co-immunoprecipitation analysis using anti-ATGL antibody and 3T3-L1 cell lysates and observed that MCT1 coprecipitated with ATGL (Figure 6I). To examine the direct interaction between MCT1 and ATGL in 3T3-L1 preadipocytes and matured 3T3-L1, we used proximity ligation assay (PLA) which identifies physical closeness of proteins (within 40 nm). We found more MCT1-ATGL interacting dots in 3T3-L1 preadipocytes than in matured adipocytes (Figure 6J; Figure S14). The frequency of MCT1-ATGL interacting dots was reversely correlated with the ATGL protein expression levels (Figure 6K), indicating that MCT1 may

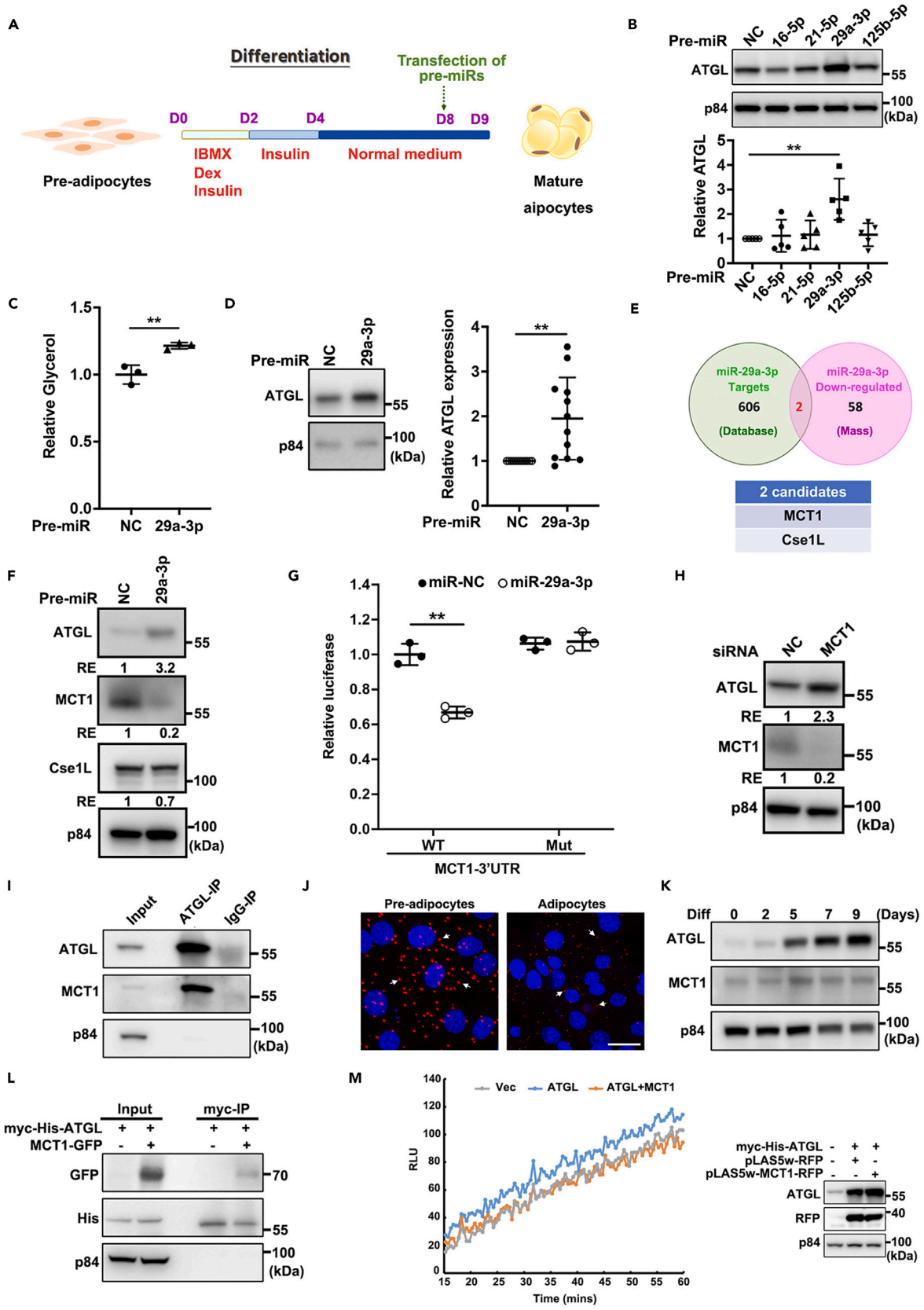
A
Differentiation
Transfection of pre-miRs
D0
D2
D4
D8
D9
IBMX
Dex
Insulin
Insulin
Normal medium
Pre-adipocytes
Mature aipocytes
B
Pre-miR
NC
16-5p
21-5p
29a-3p
125b-5p
ATGL
55
p84
100
(kDa)
Relative ATGL
**
C
Relative Glycerol
**
Pre-miR
NC
29a-3p
D
Pre-miR
NC
29a-3p
ATGL
55
p84
100
(kDa)
Relative ATGL expression
**
E
miR-29a-3p Targets
606
(Database)
2
miR-29a-3p Down-regulated
58
(Mass)
2 candidates
MCT1
Cse1L
F
Pre-miR
NC
29a-3p
ATGL
55
RE
1
3.2
MCT1
55
RE
1
0.2
Cse1L
100
RE
1
0.7
p84
100
(kDa)
G
miR-NC
miR-29a-3p
**
Relative luciferase
WT
Mut
MCT1-3'UTR
H
siRNA
NC
MCT1
ATGL
55
RE
1
2.3
MCT1
55
RE
1
0.2
p84
100
(kDa)
I
Input
ATGL-IP
IgG-IP
ATGL
55
MCT1
55
p84
100
(kDa)
J
Pre-adipocytes
Adipocytes
K
Diff
0
2
5
7
9
(Days)
ATGL
55
MCT1
55
p84
100
(kDa)
L
Input
myc-IP
myc-His-ATGL
MCT1-GFP
GFP
70
His
55
p84
100
(kDa)
M
Vec
ATGL
ATGL+MCT1
RLU
Time (mins)
myc-His-ATGL
pLAS5w-RFP
pLAS5w-MCT1-RFP
ATGL
55
RFP
40
p84
100
(kDa)

Figure 6. miR-29a-3p promotes adipose lipolysis through downregulating MCT1 expression

(A) Schema of pre-miR transfection protocol for analyzing lipolysis in 3T3-L1 cells.

(B) Upper panel: western blot of ATGL protein levels in mature 3T3-L1 adipocytes after treatment with 50 nM of miRNA-mimics for 48 h; lower panel: quantitation of the ATGL expression (n = 3).

(C) Relative amount of glycerol released into culture media in miR-29a-3p-transfected mature 3T3-L1 adipocytes (n = 3).

(D) Left panel: western blot analyses of ATGL expression in 4th mammary fat pad from C57BL/6 mice treated with miR-29a-3p mimic liposomes; Right panel shows the quantification results (n = 12), The expression of NC-injected was normalized to 1.

(E) Venn diagram of predicted miR-29a-3p target genes (using TargetScan/miRDB database) and downregulated proteins (observed in Mass analysis). Two target gene candidates—*MCT1* and *Cse1L*—were identified.

(F) Western blot analyses of ATGL, MCT1 and Cse1L expressions in 3T3-L1 adipocytes after treatment with miR-29a-3p; p84 was used as internal control.

(G) Relative luciferase activities of the luciferase plasmid constructs containing the wild-type or mutant-type 3′UTR after treatment with miR-29a-3p mimics and normalized to Renilla luciferase activity. Fold change was calculated by considering the normalized luminescence signal from pre-miR NC as "1." (**p < 0.01 versus control mimics (NC); N = 3).

(H) Western blot analyses of ATGL expression in mature 3T3-L1 adipocytes transfected with 25 nM of negative control or *MCT1* siRNA.

(I) Western blot analyses of co-immunoprecipitation of ATGL and MCT1 in mature 3T3-L1 adipocytes using antibodies against ATGL and MCT1; IgG-IP as a negative control.

(J) Proximity ligation assay (PLA) performed for ATGL and MCT1 in preadipocyte and mature 3T3-L1 adipocytes (representative images of PLA (red) and nucleus (blue) are shown; Scale bars: 25 μm.

(K) Western blot analyses of ATGL and MCT1 expressions in 3T3-L1 cells at different differentiation time points.

(L) Western blot analyses of HEK293T cells transfected with myc-His-ATGL and MCT1-GFP f and immunoprecipitated with myc-tag beads. The ATGL was blotted with anti-His tag antibody and MCT1 was blotted using anti-GFP antibody.

(M) The lipase activities of ATGL measured in lysates of HEK293T cells with/without ATGL or MCT1 expression. Lipase activity was measured for 15–60 min. Right panel shows the expression level of ATGL and MCT1-RFP (two-tailed Student's t test, *p < 0.05, **p < 0.01).

negatively regulate ATGL through direct interaction. As previous studies have found that either inhibition of MCT1[34] or overexpression of ATGL[27] can promote lipolysis, further investigation is needed to determine whether MCT1-ATGL interaction negatively regulates ATGL activity, we ectopically expressed tagged ATGL, or ATGL/MCT1 in HEK293T cells for pull-down assay and lipase activity analysis. The ectopically expressed ATGL coimmunoprecipitated with MCT1 from HEK293T cells (Figure 6L). The lipase activity (measured using fluorescent signal of EnzChek lipase substrate) increased when ATGL was overexpressed in HEK293T cells, but the increase was abolished when MCT1 was also overexpressed (Figure 6M), implicating that MCT1 is a negative regulator of ATGL via direct interaction. Collectively, these results suggest that miR-29a-3p triggers lipolysis by inhibiting MCT1 expression and consequently enhancing ATGL activity.

Exosomal miR-16-5p and miR-29a-3p directly induce adipose atrophy in mice

To further elucidate the role of exosomal miR-16-5p and miR-29a-3p *in vivo*, we established a stable Pan18 cell line lacking miR-16-5p and miR-29a-3p expression. We accomplished this by stably expressing miR-16/29-sponge which contains target sites complementary to miRNAs of interest. This miRNA sponge efficiently inhibits miRNA level without significantly affecting the properties or secretion ability of exosomes, nor does it affect cell growth under 2D conditions (Figures S15 and S16). However, we observed that using miRNA sponges to lower miRNA expression in tumor cells not only inhibited tumor growth but also alleviated cancer-induced fat loss in mice. The primary focus of our study is to investigate the genes and functions that exosomal miRNAs may regulate in adipose cells. Therefore, we then purified exosomes from culture media of Pan18 cells stably expressing empty vector or miR-16/29-sponge. These purified empty vector-exosomes and miR-16/29-sponge-exosomes were then, individually, and orbitally injected into B6 mice for 4 weeks. We found that when injected with empty vector-exosomes, the mice continued to show significant decreases in fat mass and weight of WAT, ingWAT and gWAT. However, when mice were injected with miR-16/29-sponge-exosomes, abolished the decrease in fat mass and the weight of WAT, ingWAT, and gWAT (Figures 7A–7C). These findings indicate that PDAC-exosome-induced adipose atrophy is affected mainly through exosomal miR-16-5p and miR-29a-3p.

DISCUSSION

The adipose tissue is a critical organ for systemic homeostasis of energy metabolism.[36] It secretes hormones, cytokines, and adipokines to control the energy balance of the whole body. Adipose atrophy occurs often in cancer and chronic inflammatory patients. Fat loss co-occurring with cancer is associated with shortened survival time.[10] Elevated energy expenditure, anorexia, and alterations in circulating levels of cytokine and hormones including insulin, leptin, lipid-mobilizing factor are factors that cause abnormalities in lipid metabolism, which may lead to fat loss.[37,38] Fat loss in cancer is attributed to impairment in adipogenesis[39] and elevated fat oxidation.[40] However, precise mechanism by which diseases cause adipose atrophy is poorly understood. Here, we unravel that PDAC-derived exosomal miR-16-5p and miR-29a-3p critically modulate adipose homeostasis through suppressing adipogenesis and promoting lipolysis. Mechanistically, we demonstrate that miR-16-5p and miR-29a-3p directly target *Erlin2* and *Cmpk1* expression to downregulate adipogenic genes, *C/EBPβ* and *PPARγ* while miR-29a-3p also decreases MCT1 expression to upregulate lipolytic ATGL (Figure 7D).

Fat loss is one of the major features of cancer cachexia. A growing body of literature suggests that miRNAs potentially regulate gene expression in adipose tissue.[41–43] miR-30a reduces PPAR-γ and C/EBP-α protein levels and interferes with lipid accumulation.[41] miR-155

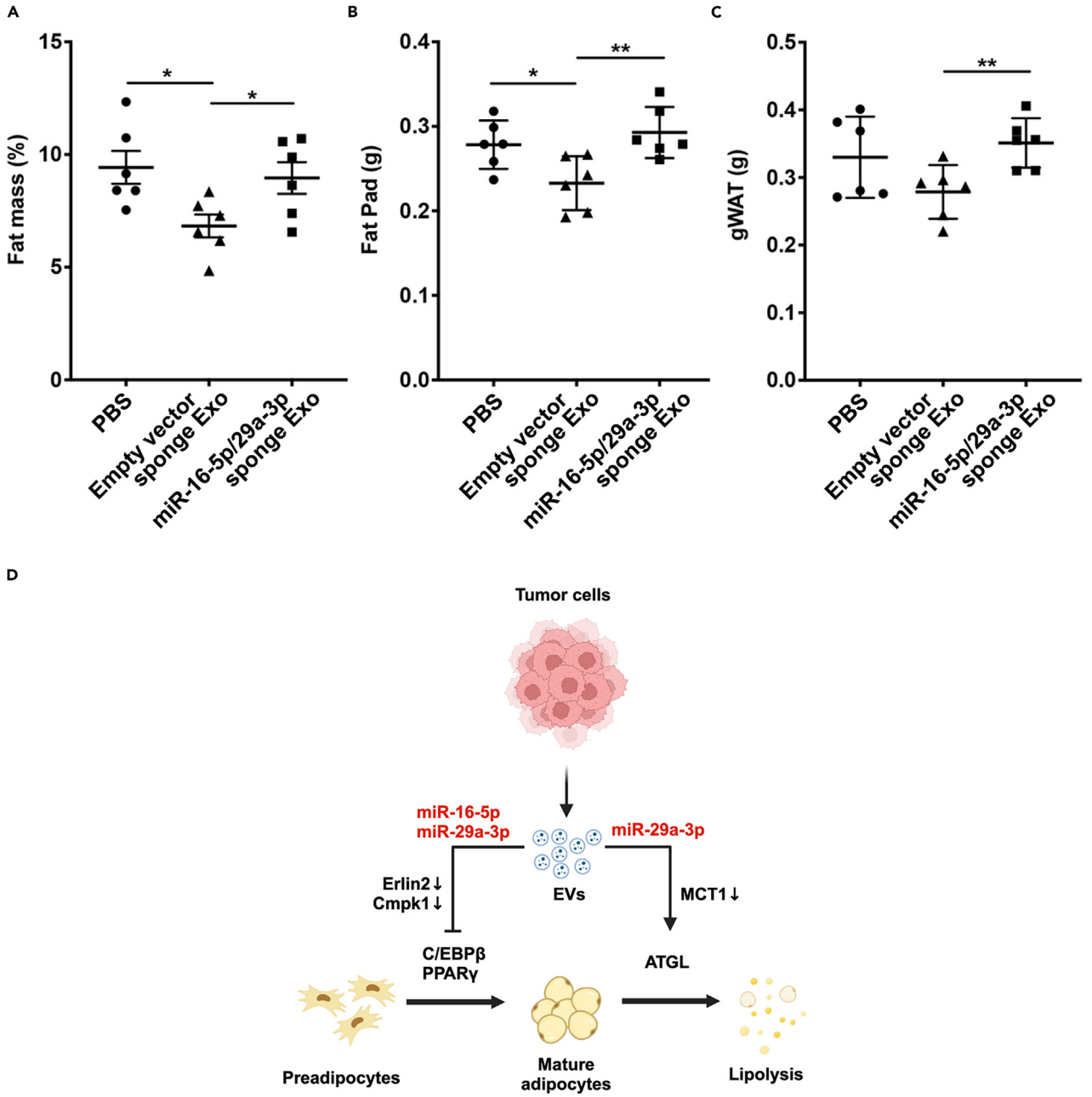

Figure 7. Ablation of miR-16-5p and miR-29a-3p in PDAC-derived exosomes restores exosome-induced fat loss in mice

Fat mass (A) and white adipose tissues (B and C) weight of C57BL/6 mice postorbitally injected daily for 4 weeks w/wo 10μg of exosomes. Exosomes were purified from culture media of Pan18 cells stably expressing empty-vector sponge or miRNA-16/miR-29a sponges. Mice injected with PBS as control. (n = 6/group; one-way ANOVA, p = 0.0298, 0.0097 and 0.0457; two-tailed Student's t test, *$p < 0.05$ and **$p < 0.01$).

(D) Proposed model: Exosomes secreted from PADC tumor cells inhibit preadipocytes differentiation and promote adipocytes lipolysis through the effects of miR-16-5p and miR-29a-3p on Erlin2, Cmpk1, and MCT1 expressions (EVs: extracellular vesicles).

enhances the catabolism in adipocytes by downregulating PPARγ.[42] miR-16-5p is overexpressed in nonobese women compared to obese women.[44] Besides, overexpression of miR-29a impairs human multipotent adipose stem (hMADS) cell differentiation[45] and negatively regulates the differentiation of porcine adipocytes by targeting *complement-C1q/tumor necrosis factor-related protein 6* (*CTRP6*), a gene that promotes adipogenesis in adipocytes.[46] Consistently, we demonstrate here, that miR-16-5p and miR-29a-3p block 3T3-L1 adipogenesis and downregulate C/EBPβ and PPARγ expression (Figure 5). Furthermore, we identify that miR-16-5p and miR-29a-3p directly target *Erlin2*

and *Cmpk1* genes in regulating early adipocyte differentiation (Figures 5G–5J; Figure S11). In addition, silencing or ectopically expressing *Erlin2* and *Cmpk1* can, respectively, diminish or augment C/EBPβ and PPARγ expression (Figures 5K and 5L), suggesting that Erlin2 and Cmpk1 are upstream regulators of adipogenesis. These findings reveal a surprisingly nuanced adipogenesis process with a fine-tuning machinery. However, it remains intriguing how these two factors participate in the adipogenesis cascade. Erlin2 supports cancer cell growth by regulating cytosolic lipid droplet production in response to insulin through activating sterol regulatory element binding protein-1c (SREBP-1c),[32] an inducer of adipogenesis. Meanwhile, Cmpk1 is importantly involved in *de novo* pyrimidine nucleotide biosynthesis.[47] Further, WAT from high-fat diet fed mice contains higher nucleotides cytidine-5′-monophosphate (CMP) and uridine monophosphate (UMP),[33] suggesting a functional relevance for pyrimidine intermediates in diet-dependent adipose tissue metabolism. However, the exact mechanism by which Erlin2 and Cmpk1 modulate C/EBPβ and PPARγ expression during adipocyte differentiation remains unclarified.

To explore whether tumors induce a reduction in fat cells through exosomes, we knocked down Rab27 in Pan18 cells to decrease the tumor cells' exosome secretion capacity. As depicted in Figure S4, we observed that Rab27 KD Pan18 cells did not induce a decrease in fat cells. However, the tumor cell size of Rab27KD Pan18 was notably smaller compared to the LacZ group. Previous studies have highlighted that Rab27, as a member of the GTPase family, can modulate various downstream effectors, thus exhibiting certain oncogenic properties.[48] Its expression levels have the potential to serve as prognostic indicators. This association suggests that Rab27 not only affects exosome secretion but also correlates with cancer progression and metastasis.[49] In addition, RAB27A was identified as an oncogene in melanoma, promoting cell proliferation through the ERK pathway.[50] Similarly, RAB27B has been shown to regulate MAPK and VEGF signaling independent of exosome function.[51] These findings suggest that Rab27 knockdown in PDAC cells could also influence other signaling pathways, potentially contributing to slower tumor growth *in vivo* models.

The biodistribution of fluorescent exosomes in mice administered via orbital injection revealed that, in addition to being absorbed by adipose tissues, the majority of exosomes can also be localized in the liver (Figure 2B). This is consistent with previous studies, which suggest that irrespective of the injection route, the liver tends to be the primary organ for exosome uptake.[52] Adipose tissue and the liver play significant roles in regulating whole-body energy homeostasis. Therefore, we cannot entirely rule out the possibility of exosomes being absorbed by the liver and affecting fat metabolism. Lipolysis also plays a central role in the regulation of cancer-induced atrophy.[53] Our results revealed that miR-29a-3p not only increases expression of ATGL, a rate-limiting enzyme of lipolysis, but induces glycerol release from adipocytes (Figure 6). Although, ablation of ATGL protects mice from cancer-associated weight loss and adipose tissue loss, the molecular pathway behind this effect is unknown.[54] Here, using mass spectrometry and miRNA database analysis, we found that MCT1 and Cse1L are the targets of miR-29a-3p. Moreover, miR-29a-3p increases lipolysis through decreasing MCT1 and leading to ATGL upregulation (Figures 6E–6H). It is very intriguing how MCT (an importer of monocarboxylates, such as lactate and pyruvate) negatively modulates ATGL. Perilipin-5 interacts with ATGL and inhibits ATGL activity by restricting its physical access to lipid droplets (LDs).[55] Like perilipin-5, we found that MCT1 binds to ATGL and inhibits ATGL activity (Figure 6). However, the precise mechanism by which MCT1 reduces the expression and activity of ATGL remains to be elucidated.

To verify whether tumor cell inoculation leads to increased miRNA expression and influences overall gene alterations in mice, we orthotopically injected mPDAC Pan18 cells in to mice and analyzed miRNA expression in adipose tissue, 1–3 weeks after tumor cell inoculation. RNAscope of WAT (Figure S17A) from control and PDAC-implanted mice, revealed that the expression levels of miR-16-5p and miR-29a-3p peaked in the second week and gradually declined, thereafter. This trend was also confirmed by qPCR results (Figure S17B). The decrease in miR expression during the third week might be attributed to common mechanisms—depletion, degradation, or utilization—by which cells regulate miRNA levels to ensure proper gene expression and cellular functions. Another possibility is that the relatively lower levels of miRNA detected in adipose cells three weeks after tumor cell injection may be due to the initiation of adipocyte shrinkage during this period, which could pose a challenge in detecting the accumulation of miRNA in adipose tissues. These findings validate our hypothesis that Pan18 tumor cells indeed release miR-16-5p and miR-29a-3p, which are likely taken up by adipose tissue, where they subsequently affect the expression of target genes. Through RNA-seq analysis, we observed that the expression of predicted target genes (*Erlin2*, *Cmpk1*, *MCT1*) are indeed lower in Pan18 group (Figure S17C).

Circulating exosomal miRNAs play multiple functions in cancer progression and serve as candidate biomarkers and therapeutic targets. miR-29a-3p is enriched in the exosomes derived from tumor-associated macrophages, which regulate immunity and affect the progression of ovarian cancer.[56] miR-125b-5p is associated with metastasis in pancreatic cancer[57] and serum exosomal miR-125b could serve as a promising prognostic marker for hepatocellular carcinoma.[58] Exosomal miR-21 is overexpressed in pancreatic cancer.[59] Moreover, the activated pancreatic stellate cells continuously release miR-21-enriched exosomes that are endocytosed by pancreatic cancer cells.[60] Once inside cancer cells, the abundant miR-21 activates RAS/ERK signaling and induces epithelial-to-mesenchymal transition (EMT).[60] Interestingly, we found that exosomal miR-16-5p, miR-21-5p, miR-29a-3p, and miR-125b-5p are highly expressed in culture media of PDAC cells and serum of mice or patients with PDAC tumor (Figure 4). Further, exosomal miR-16-5p and miR-29a-3p play major roles in PDAC-induced fat loss through inhibiting adipogenesis and promoting lipolysis (Figure 7). Although the effects of miR-21/miR-125b-5p on fat loss are not clear, these exosomal miRNAs may have roles in metastasis and malignancy of pancreatic cancer and must be further investigated.

Adipose tissues are known targets in cachexia therapy, but clinical proof is lacking.[38] Our findings, pave way for exploration of new therapies—that can block adipose tissue atrophy by inhibiting exosomal miR-16-5p and miR-29a-3p—for treating cancer cachexia.

In summary, our findings highlight the importance of exosomal miR-16-5p and miR-29a-3p in adipose tissue metabolism, which they modulate via establishing cellular communication between tumor cells and adipose tissues. Manipulating miRNAs content in exosomes to reprogram lipid metabolism is a potential strategy for developing new therapy for obesity and cancer cachexia.

Limitations of the study

This study has several limitations. First, obtaining patient samples, especially pre-diagnostic ones, presents a significant challenge. While longitudinal studies with such samples would ideally enable a more comprehensive analysis of the relationship between exosomal miR-16-5p and miR-29a-3p expression and the development of cachexia in PDAC patients, acquiring these samples and relevant clinical data (e.g., BMI, CT scans) before diagnosis is often unfeasible in clinical practice. This limitation hinders comparisons with the post-diagnosis state.

Second, this study primarily focused on establishing potential roles for these exosomal miRNAs in adipose atrophy. While our findings suggest a link to cachexia, further *in vivo* functional validation is necessary to definitively demonstrate the impact of miR-16-5p and miR-29a-3p on metastasis and survival rates. Future research utilizing techniques such as Rab27 knockdown and miRNA sponges in animal models could elucidate these potential effects.

STAR★METHODS

Detailed methods are provided in the online version of this paper and include the following:

- KEY RESOURCES TABLE
- RESOURCE AVAILABILITY
  - Lead contact
  - Materials availability
  - Data and code availability
- EXPERIMENTAL MODEL AND STUDY PARTICIPANT DETAILS
  - Ethics statement
  - Human specimens
  - Animal protocols, diets, and treatment
  - Sample size estimation
  - General cell culture and establishment of stable cell lines
  - Establishment of syngeneic and xenograft mouse models
  - Mouse primary pancreatic acinar cell culture
- METHOD DETAILS
  - Plasmids and transfections
  - Protein extraction and western blotting analysis
  - RNA extraction and quantitative real-time PCR
  - Histology and quantification of adipose tissues
  - Purification of exosomes from conditioned medium
  - Isolation of exosomes from human plasma and mouse serum
  - Nanoparticle Tracking Analysis (NTA)
  - TEM and Cryo-EM
  - Bio-distribution of exosomes
  - Body composition measurement
  - Differentiation of pre-adipocyte 3T3-L1
  - Glycerol assay
  - Oil red staining
  - Immunoprecipitation
  - ATGL lipase activity assay
  - Small RNA-seq
  - In-vivo miRNA delivery
  - Dual-luciferase reporter assay
  - LC-MS/MS analysis
  - *In situ* proximity ligation assay (PLA)
- QUANTIFICATION AND STATISTICAL ANALYSIS
  - Statistical analysis

SUPPLEMENTAL INFORMATION

Supplemental information can be found online at https://doi.org/10.1016/j.isci.2024.110346.

ACKNOWLEDGMENTS

We thank Dr. Chia-Ning Shen for Pan18 cells and Dr. Shine-Gwo Shiah for pmiR-Glo vector, GRC Mass Core Facility at Academia Sinica in Taiwan for mass analysis, the National RNAi Core Facility at Academia Sinica in Taiwan for providing shRNA plasmids, the Taiwan Mouse

Clinic, Academia Sinica, and Taiwan Animal Consortium for the technical support in body composition, and GRC/AS Animal Core Facility at Academia Sinica in Taiwan for providing animal support. This work was supported by National Health Research Institutes of Taiwan (NHRI-EX111-11123BI), Academia Sinica of Taiwan (AS-GC-110-MD03, AS-KPQ-111-KNT) and National Science and Technology Council of Taiwan (NSTC112-2326-B-001-007, NSTC 113-2634-F-039-001).

AUTHOR CONTRIBUTIONS

S.C.T., W.H.L., and C.M.H. designed the experiments. S.C.T. performed most of the experiments with assistance from C.C.C., C.H.H., and H.Y.P. S.C.T., C.C.C., and C.M.H. analyzed the data. Y.T.C. and M.C.C. were responsible for collecting the clinical samples. Finally, S.C.T. and C.M.H. wrote the manuscript, with C.M.H. overseeing the entire project.

DECLARATION OF INTERESTS

The authors declare no competing interests.

Received: January 30, 2024
Revised: April 20, 2024
Accepted: June 19, 2024
Published: June 21, 2024

REFERENCES

1. Ryan, D.P., Hong, T.S., and Bardeesy, N. (2014). Pancreatic adenocarcinoma. N. Engl. J. Med. *371*, 1039–1049. https://doi.org/10.1056/NEJMra1404198.
2. Ducreux, M., Cuhna, A.S., Caramella, C., Hollebecque, A., Burtin, P., Goéré, D., Seufferlein, T., Haustermans, K., Van Laethem, J.L., Conroy, T., et al. (2015). Cancer of the pancreas: ESMO Clinical Practice Guidelines for diagnosis, treatment and follow-up. Ann. Oncol. *26*, v56–v68. https://doi.org/10.1093/annonc/mdv295.
3. Baracos, V.E., Martin, L., Korc, M., Guttridge, D.C., and Fearon, K.C.H. (2018). Cancer-associated cachexia. Nat. Rev. Dis. Primers *4*, 17105. https://doi.org/10.1038/nrdp.2017.105.
4. Biswas, A.K., and Acharyya, S. (2020). Understanding cachexia in the context of metastatic progression. Nat. Rev. Cancer *20*, 274–284. https://doi.org/10.1038/s41568-020-0251-4.
5. Fearon, K., Arends, J., and Baracos, V. (2013). Understanding the mechanisms and treatment options in cancer cachexia. Nat. Rev. Clin. Oncol. *10*, 90–99. https://doi.org/10.1038/nrclinonc.2012.209.
6. Mulder, S.E., Dasgupta, A., King, R.J., Abrego, J., Attri, K.S., Murthy, D., Shukla, S.K., and Singh, P.K. (2020). JNK signaling contributes to skeletal muscle wasting and protein turnover in pancreatic cancer cachexia. Cancer Lett. *491*, 70–77. https://doi.org/10.1016/j.canlet.2020.07.025.
7. Poulia, K.A., Sarantis, P., Antoniadou, D., Koustas, E., Papadimitropoulou, A., Papavassiliou, A.G., and Karamouzis, M.V. (2020). Pancreatic Cancer and Cachexia-Metabolic Mechanisms and Novel Insights. Nutrients *12*, 1543. https://doi.org/10.3390/nu12061543.
8. Bonetto, A., Aydogdu, T., Jin, X., Zhang, Z., Zhan, R., Puzis, L., Koniaris, L.G., and Zimmers, T.A. (2012). JAK/STAT3 pathway inhibition blocks skeletal muscle wasting downstream of IL-6 and in experimental cancer cachexia. Am. J. Physiol. Endocrinol. Metab. *303*, E410–E421. https://doi.org/10.1152/ajpendo.00039.2012.
9. Pezzilli, R., Caccialanza, R., Capurso, G., Brunetti, O., Milella, M., and Falconi, M. (2020). Pancreatic Enzyme Replacement Therapy in Pancreatic Cancer. Cancers *12*, 275. https://doi.org/10.3390/cancers12020275.
10. Murphy, R.A., Wilke, M.S., Perrine, M., Pawlowicz, M., Mourtzakis, M., Lieffers, J.R., Maneshgar, M., Bruera, E., Clandinin, M.T., Baracos, V.E., and Mazurak, V.C. (2010). Loss of adipose tissue and plasma phospholipids: relationship to survival in advanced cancer patients. Clin. Nutr. *29*, 482–487. https://doi.org/10.1016/j.clnu.2009.11.006.
11. Fouladiun, M., Körner, U., Bosaeus, I., Daneryd, P., Hyltander, A., and Lundholm, K.G. (2005). Body composition and time course changes in regional distribution of fat and lean tissue in unselected cancer patients on palliative care–correlations with food intake, metabolism, exercise capacity, and hormones. Cancer *103*, 2189–2198. https://doi.org/10.1002/cncr.21013.
12. Rohm, M., Zeigerer, A., Machado, J., and Herzig, S. (2019). Energy metabolism in cachexia. EMBO Rep. *20*, e47258. https://doi.org/10.15252/embr.201847258.
13. Rydén, M., Agustsson, T., Laurencikiene, J., Britton, T., Sjolin, E., Isaksson, B., Permert, J., and Arner, P. (2008). Lipolysis–not inflammation, cell death, or lipogenesis–is involved in adipose tissue loss in cancer cachexia. Cancer *113*, 1695–1704. https://doi.org/10.1002/cncr.23802.
14. Agustsson, T., Rydén, M., Hoffstedt, J., van Harmelen, V., Dicker, A., Laurencikiene, J., Isaksson, B., Permert, J., and Arner, P. (2007). Mechanism of increased lipolysis in cancer cachexia. Cancer Res. *67*, 5531–5537. https://doi.org/10.1158/0008-5472.CAN-06-4585.
15. Ebadi, M., and Mazurak, V.C. (2014). Evidence and mechanisms of fat depletion in cancer. Nutrients *6*, 5280–5297. https://doi.org/10.3390/nu6115280.
16. Jafari, N., Llevenes, P., and Denis, G.V. (2022). Exosomes as novel biomarkers in metabolic disease and obesity-related cancers. Nat. Rev. Endocrinol. *18*, 327–328. https://doi.org/10.1038/s41574-022-00666-7.
17. De Toro, J., Herschlik, L., Waldner, C., and Mongini, C. (2015). Emerging roles of exosomes in normal and pathological conditions: new insights for diagnosis and therapeutic applications. Front. Immunol. *6*, 203. https://doi.org/10.3389/fimmu.2015.00203.
18. Arroyo, J.D., Chevillet, J.R., Kroh, E.M., Ruf, I.K., Pritchard, C.C., Gibson, D.F., Mitchell, P.S., Bennett, C.F., Pogosova-Agadjanyan, E.L., Stirewalt, D.L., et al. (2011). Argonaute2 complexes carry a population of circulating microRNAs independent of vesicles in human plasma. Proc. Natl. Acad. Sci. USA *108*, 5003–5008. https://doi.org/10.1073/pnas.1019055108.
19. Filipowicz, W., Bhattacharyya, S.N., and Sonenberg, N. (2008). Mechanisms of post-transcriptional regulation by microRNAs: are the answers in sight? Nat. Rev. Genet. *9*, 102–114. https://doi.org/10.1038/nrg2290.
20. Momen-Heravi, F., Getting, S.J., and Moschos, S.A. (2018). Extracellular vesicles and their nucleic acids for biomarker discovery. Pharmacol. Ther. *192*, 170–187. https://doi.org/10.1016/j.pharmthera.2018.08.002.
21. Argilés, J.M., Stemmler, B., Lopez-Soriano, F.J., and Busquets, S. (2018). Inter-tissue communication in cancer cachexia. Nat. Rev. Endocrinol. *15*, 9–20. https://doi.org/10.1038/s41574-018-0123-0.
22. Rupert, J.E., Narasimhan, A., Jengelley, D.H.A., Jiang, Y., Liu, J., Au, E., Silverman, L.M., Sandusky, G., Bonetto, A., Cao, S., et al. (2021). Tumor-derived IL-6 and trans-signaling among tumor, fat, and muscle mediate pancreatic cancer cachexia. J. Exp. Med. *218*, e20190450. https://doi.org/10.1084/jem.20190450.
23. Chen, Y.L., Hu, C.M., Hsu, J.T., Chang, C.C., Huang, T.Y., Chiang, P.H., Chen, W.Y., Chang, Y.T., Chang, M.C., Tien, Y.W., et al. (2018). Cellular 5-hydroxylmethylcytosine content determines tumorigenic potential and prognosis of pancreatic ductal adenocarcinoma. Am. J. Cancer Res. *8*, 2548–2563.
24. Tkach, M., and Théry, C. (2016). Communication by Extracellular

Vesicles: Where We Are and Where We Need to Go. Cell *164*, 1226–1232. https://doi.org/10.1016/j.cell.2016.01.043.
25. Ostrowski, M., Carmo, N.B., Krumeich, S., Fanget, I., Raposo, G., Savina, A., Moita, C.F., Schauer, K., Hume, A.N., Freitas, R.P., et al. (2010). Rab27a and Rab27b control different steps of the exosome secretion pathway. Nat. Cell Biol. *12*, 19–30. sup pp 11-13. https://doi.org/10.1038/ncb2000.
26. Thery, C., Amigorena, S., Raposo, G., and Clayton, A. (2006). Isolation and characterization of exosomes from cell culture supernatants and biological fluids. Curr. Protoc. Cell Biol. *Chapter 3*. Unit 3.22. https://doi.org/10.1002/0471143030.cb0322s30.
27. Miyoshi, H., Perfield, J.W., Obin, M.S., and Greenberg, A.S. (2008). Adipose triglyceride lipase regulates basal lipolysis and lipid droplet size in adipocytes. J. Cell. Biochem. *105*, 1430–1436. https://doi.org/10.1002/jcb.21964.
28. Zechner, R., Kienesberger, P.C., Haemmerle, G., Zimmermann, R., and Lass, A. (2009). Adipose triglyceride lipase and the lipolytic catabolism of cellular fat stores. J. Lipid Res. *50*, 3–21. https://doi.org/10.1194/jlr.R800031-JLR200.
29. Petruzzelli, M., Schweiger, M., Schreiber, R., Campos-Olivas, R., Tsoli, M., Allen, J., Swarbrick, M., Rose-John, S., Rincon, M., Robertson, G., et al. (2014). A switch from white to brown fat increases energy expenditure in cancer-associated cachexia. Cell Metab. *20*, 433–447. https://doi.org/10.1016/j.cmet.2014.06.011.
30. Ramírez-Zacarias, J.L., Castro-Munozledo, F., and Kuri-Harcuch, W. (1992). Quantitation of adipose conversion and triglycerides by staining intracytoplasmic lipids with Oil red O. Histochemistry *97*, 493–497. https://doi.org/10.1007/BF00316069.
31. Lefterova, M.I., Zhang, Y., Steger, D.J., Schupp, M., Schug, J., Cristancho, A., Feng, D., Zhuo, D., Stoeckert, C.J., Jr., Liu, X.S., and Lazar, M.A. (2008). PPARgamma and C/EBP factors orchestrate adipocyte biology via adjacent binding on a genome-wide scale. Genes Dev. *22*, 2941–2952. https://doi.org/10.1101/gad.1709008.
32. Wang, G., Zhang, X., Lee, J.S., Wang, X., Yang, Z.Q., and Zhang, K. (2012). Endoplasmic reticulum factor ERLIN2 regulates cytosolic lipid content in cancer cells. Biochem. J. *446*, 415–425. https://doi.org/10.1042/BJ20112050.
33. Cummins, T.D., Holden, C.R., Sansbury, B.E., Gibb, A.A., Shah, J., Zafar, N., Tang, Y., Hellmann, J., Rai, S.N., Spite, M., et al. (2014). Metabolic remodeling of white adipose tissue in obesity. Am. J. Physiol. Endocrinol. Metab. *307*, E262–E277. https://doi.org/10.1152/ajpendo.00271.2013.
34. Bailey, T., Nieto, A., and McDonald, P. (2022). Inhibition of the Monocarboxylate Transporter 1 (MCT1) Promotes 3T3-L1 Adipocyte Proliferation and Enhances Insulin Sensitivity. Int. J. Mol. Sci. *23*, 1901. https://doi.org/10.3390/ijms23031901.
35. Zhang, X., Zhang, X., Mao, T., Xu, H., Cui, J., Lin, H., and Wang, L. (2021). CSE1L, as a novel prognostic marker, promotes pancreatic cancer proliferation by regulating the AKT/mTOR signaling pathway. J. Cancer *12*, 2797–2806. https://doi.org/10.7150/jca.54482.
36. Choe, S.S., Huh, J.Y., Hwang, I.J., Kim, J.I., and Kim, J.B. (2016). Adipose Tissue Remodeling: Its Role in Energy Metabolism and Metabolic Disorders. Front. Endocrinol. *7*, 30. https://doi.org/10.3389/fendo.2016.00030.
37. Tisdale, M.J. (2002). Cachexia in cancer patients. Nat. Rev. Cancer *2*, 862–871. https://doi.org/10.1038/nrc927.
38. Sun, X., Feng, X., Wu, X., Lu, Y., Chen, K., and Ye, Y. (2020). Fat Wasting Is Damaging: Role of Adipose Tissue in Cancer-Associated Cachexia. Front. Cell Dev. Biol. *8*, 33. https://doi.org/10.3389/fcell.2020.00033.
39. Bing, C., Russell, S., Becket, E., Pope, M., Tisdale, M.J., Trayhurn, P., and Jenkins, J.R. (2006). Adipose atrophy in cancer cachexia: morphologic and molecular analysis of adipose tissue in tumour-bearing mice. Br. J. Cancer *95*, 1028–1037. https://doi.org/10.1038/sj.bjc.6603360.
40. Zuijdgeest-van Leeuwen, S.D., van den Berg, J.W., Wattimena, J.L., van der Gaast, A., Swart, G.R., Wilson, J.H., and Dagnelie, P.C. (2000). Lipolysis and lipid oxidation in weight-losing cancer patients and healthy subjects. Metabolism *49*, 931–936. https://doi.org/10.1053/meta.2000.6740.
41. Li, K., Wu, Y., Yang, H., Hong, P., Fang, X., and Hu, Y. (2019). H19/miR-30a/C8orf4 axis modulates the adipogenic differentiation process in human adipose tissue-derived mesenchymal stem cells. J. Cell. Physiol. *234*, 20925–20934. https://doi.org/10.1002/jcp.28697.
42. Wu, Q., Sun, S., Li, Z., Yang, Q., Li, B., Zhu, S., Wang, L., Wu, J., Yuan, J., Yang, C., et al. (2018). Tumour-originated exosomal miR-155 triggers cancer-associated cachexia to promote tumour progression. Mol. Cancer *17*, 155. https://doi.org/10.1186/s12943-018-0899-5.
43. Zhang, X., Liu, L., Dou, C., Cheng, P., Liu, L., Liu, H., Ren, S., Wang, C., Jia, S., Chen, L., et al. (2019). PPAR Gamma-Regulated MicroRNA 199a-5p Underlies Bone Marrow Adiposity in Aplastic Anemia. Mol. Ther. Nucleic Acids *17*, 678–687. https://doi.org/10.1016/j.omtn.2019.07.005.
44. Gasparotto, A.S., Borges, D.O., Sassi, M.G.M., Milani, A., Rech, D.L., Terres, M., Ely, P.B., Ramos, M.J., Meihnardt, N.G., and Mattevi, V.S. (2019). Differential expression of miRNAs related to angiogenesis and adipogenesis in subcutaneous fat of obese and nonobese women. Mol. Biol. Rep. *46*, 965–973. https://doi.org/10.1007/s11033-018-4553-5.
45. Glantschnig, C., Koenen, M., Gil-Lozano, M., Karbiener, M., Pickrahn, I., Williams-Dautovich, J., Patel, R., Cummins, C.L., Giroud, M., Hartleben, G., et al. (2019). A miR-29a-driven negative feedback loop regulates peripheral glucocorticoid receptor signaling. FASEB J. *33*, 5924–5941. https://doi.org/10.1096/fj.201801385RR.
46. Wu, W., Zhang, J., Zhao, C., Sun, Y., Pang, W., and Yang, G. (2017). CTRP6 Regulates Porcine Adipocyte Proliferation and Differentiation by the AdipoR1/MAPK Signaling Pathway. J. Agric. Food Chem. *65*, 5512–5522. https://doi.org/10.1021/acs.jafc.7b00594.
47. Chu, H., Han, N., and Xu, J. (2021). CMPK1 Regulated by miR-130b Attenuates Response to 5-FU Treatment in Gastric Cancer. Front. Oncol. *11*, 637470. https://doi.org/10.3389/fonc.2021.637470.
48. Li, Z., Fang, R., Fang, J., He, S., and Liu, T. (2018). Functional implications of Rab27 GTPases in Cancer. Cell Commun. Signal. *16*, 44. https://doi.org/10.1186/s12964-018-0255-9.
49. Koh, H.M., Jang, B.G., and Kim, D.C. (2020). Prognostic significance of Rab27 expression in solid cancer: a systematic review and meta-analysis. Sci. Rep. *10*, 14136. https://doi.org/10.1038/s41598-020-71104-9.
50. Laughlin, K.M., Luo, D., Liu, C., Shaw, G., Warrington, K.H., Jr., Law, B.K., and Harrison, J.K. (2009). Hematopoietic- and neurologic-expressed sequence 1 (Hn1) depletion in B16.F10 melanoma cells promotes a differentiated phenotype that includes increased melanogenesis and cell cycle arrest. Differentiation *78*, 35–44. https://doi.org/10.1016/j.diff.2009.04.001.
51. Tsuruda, M., Yoshino, H., Okamura, S., Kuroshima, K., Osako, Y., Sakaguchi, T., Sugita, S., Tatarano, S., Nakagawa, M., and Enokida, H. (2020). Oncogenic effects of RAB27B through exosome independent function in renal cell carcinoma including sunitinib-resistant. PLoS One *15*, e0232545. https://doi.org/10.1371/journal.pone.0232545.
52. Kang, M., Jordan, V., Blenkiron, C., and Chamley, L.W. (2021). Biodistribution of extracellular vesicles following administration into animals: A systematic review. J. Extracell. Vesicles *10*, e12085. https://doi.org/10.1002/jev2.12085.
53. Petruzzelli, M., and Wagner, E.F. (2016). Mechanisms of metabolic dysfunction in cancer-associated cachexia. Genes Dev. *30*, 489–501. https://doi.org/10.1101/gad.276733.115.
54. Das, S.K., Eder, S., Schauer, S., Diwoky, C., Temmel, H., Guertl, B., Gorkiewicz, G., Tamilarasan, K.P., Kumari, P., Trauner, M., et al. (2011). Adipose triglyceride lipase contributes to cancer-associated cachexia. Science *333*, 233–238. https://doi.org/10.1126/science.1198973.
55. Wang, H., Bell, M., Sreenivasan, U., Sreenevasan, U., Hu, H., Liu, J., Dalen, K., Londos, C., Yamaguchi, T., Rizzo, M.A., et al. (2011). Unique regulation of adipose triglyceride lipase (ATGL) by perilipin 5, a lipid droplet-associated protein. J. Biol. Chem. *286*, 15707–15715. https://doi.org/10.1074/jbc.M110.207779.
56. Lu, L., Ling, W., and Ruan, Z. (2021). TAM-derived extracellular vesicles containing microRNA-29a-3p explain the deterioration of ovarian cancer. Mol. Ther. Nucleic Acids *25*, 468–482. https://doi.org/10.1016/j.omtn.2021.05.011.
57. Wu, M., Tan, X., Liu, P., Yang, Y., Huang, Y., Liu, X., Meng, X., Yu, B., Wu, Y., and Jin, H. (2020). Role of exosomal microRNA-125b-5p in conferring the metastatic phenotype among pancreatic cancer cells with different potential of metastasis. Life Sci. *255*, 117857. https://doi.org/10.1016/j.lfs.2020.117857.
58. Liu, W., Hu, J., Zhou, K., Chen, F., Wang, Z., Liao, B., Dai, Z., Cao, Y., Fan, J., and Zhou, J. (2017). Serum exosomal miR-125b is a novel prognostic marker for hepatocellular carcinoma. OncoTargets Ther. *10*, 3843–3851. https://doi.org/10.2147/OTT.S140062.
59. Que, R., Ding, G., Chen, J., and Cao, L. (2013). Analysis of serum exosomal microRNAs and clinicopathologic features of patients with pancreatic adenocarcinoma. World J. Surg. Oncol. *11*, 219. https://doi.org/10.1186/1477-7819-11-219.
60. Ma, Q., Wu, H., Xiao, Y., Liang, Z., and Liu, T. (2020). Upregulation of exosomal microRNA21 in pancreatic stellate cells

promotes pancreatic cancer cell migration and enhances Ras/ERK pathway activity. Int. J. Oncol. *56*, 1025–1033. https://doi.org/10.3892/ijo.2020.4986.

61. Ouyang, H., Mou, L., Luk, C., Liu, N., Karaskova, J., Squire, J., and Tsao, M.S. (2000). Immortal human pancreatic duct epithelial cell lines with near normal genotype and phenotype. Am. J. Pathol. *157*, 1623–1631. https://doi.org/10.1016/S0002-9440(10)64800-6.
62. Shen, C.N., Goh, K.S., Huang, C.R., Chiang, T.C., Lee, C.Y., Jeng, Y.M., Peng, S.J., Chien, H.J., Chung, M.H., Chou, Y.H., et al. (2019). Lymphatic vessel remodeling and invasion in pancreatic cancer progression. EBioMedicine *47*, 98–113. https://doi.org/10.1016/j.ebiom.2019.08.044.
63. Rucki, A.A., Xiao, Q., Muth, S., Chen, J., Che, X., Kleponis, J., Sharma, R., Anders, R.A., Jaffee, E.M., and Zheng, L. (2017). Dual Inhibition of Hedgehog and c-Met Pathways for Pancreatic Cancer Treatment. Mol. Cancer Ther. *16*, 2399–2409. https://doi.org/10.1158/1535-7163.MCT-16-0452.
64. Gout, J., Pommier, R.M., Vincent, D.F., Kaniewski, B., Martel, S., Valcourt, U., and Bartholin, L. (2013). Isolation and culture of mouse primary pancreatic acinar cells. J. Vis. Exp. *78*, 50514. https://doi.org/10.3791/50514.
65. Iglesias, J., Lamontagne, J., Erb, H., Gezzar, S., Zhao, S., Joly, E., Truong, V.L., Skorey, K., Crane, S., Madiraju, S.R.M., and Prentki, M. (2016). Simplified assays of lipolysis enzymes for drug discovery and specificity assessment of known inhibitors. J. Lipid Res. *57*, 131–141. https://doi.org/10.1194/jlr.D058438.

STAR★METHODS

KEY RESOURCES TABLE

REAGENT or RESOURCE	SOURCE	IDENTIFIER
Antibodies		
Anti-Alix	Abcam	Cat# ab186429; RRID: AB_2754981
Anti-UCP1	Abcam	Cat# ab10983; RRID: AB_2241462
Anti-CD81	Santa Cruz	Cat# sc-166029; RRID: AB_2275892
anti-C/EBPβ	BioLegend	Cat# 606202; RRID: AB_315675
anti-TSG101	GeneTex	Cat# GTX70255; RRID: AB_373239
anti-Erlin2	GeneTex	Cat# GTX106277; RRID: AB_1950226
anti-CMPK1	GeneTex	Cat# GTX105566; RRID: AB_1950004
anti-MCT1	GeneTex	Cat# GTX631643; RRID: AB_2888249
anti-Cse1L	GeneTex	Cat# GTX103005; RRID: AB_1950046
anti-RFP	GeneTex	Cat# GTX127897; RRID: AB_2885652
anti-GAPDH	GeneTex	Cat# GTX100118; RRID: AB_1080976
Anti-p84	GeneTex	Cat# GTX70220; RRID: AB_372637
anti-Rab27a	Proteintech	Cat# Cat:17817-1-AP; RRID: AB_2176728
anti-Rab27b	Proteintech	Cat# Cat:13412-1-AP; RRID: AB_2176732
anti-ATGL	Cell Signaling Technology	Cat# 2138; RRID: AB_2167955
anti-PPARγ	Cell Signaling Technology	Cat# 2443; RRID: AB_823598
HRP goat anti-mouse	Jackson ImmunoResearch	Cat# 111-035-146; RRID: AB_2307392
HRP goat anti-rabbit	Jackson ImmunoResearch	Cat# 111-035-144; RRID: AB_2307391
Chemicals, peptides, and recombinant proteins		
Hoechst 33342	Sigma-Aldrich	Cat# B2261
HBSS	Sigma-Aldrich	Cat# H6648
HEPES	Sigma-Aldrich	Cat# H4034
Collagenase IA	Sigma-Aldrich	Cat# C0130
Dexamethasone	Sigma-Aldrich	Cat# D4902
Isobutyl-methylxanthine	Sigma-Aldrich	Cat# I7018
Oil Red O	Sigma-Aldrich	Cat# O0625
EGF	Thermo Fisher	Cat# PHG0311
Soybean Trypsin inhibitor	Thermo Fisher	Cat# 17075029
DiR dye	Invitrogen	Cat# D12731
Passive Lysis Buffer	Promega	Cat# E1910
jetPEI transfection regent	Polyplus	Cat# 201-50G
EnzChek lipase substrate, green fluorescence	Invitrogen	Cat# E33955
TRIzol	Thermo Fisher	Cat# 15596026
TRIzol, LS	Thermo Fisher	Cat# 10296028
SYBR Green	ABI	Cat# KK4603
DMEM	Gibco	Cat# 11965-092
RPMI1640	Gibco	Cat# 22400-089
Exosome-depleted FBS	Gibco	Cat# A2720801
Critical commercial assays		
Glycerol assay kit	Sigma-Aldrich	Cat# MAK-117

(*Continued on next page*)

Continued

REAGENT or RESOURCE	SOURCE	IDENTIFIER
Total Exosome Isolation reagent (from serum)	Thermo Fisher	Cat# 4478360
miScript II RT kit	Qiagen	Cat# 218161
Dual-Glo Luciferase assay system	Promega	Cat# E2920
Deposited data		
mass spectrometry proteomics data	This paper	PXD037862 and PXD037998
Small RNA-seq data	This paper	Accession codes: SRR22103074 to SRR22103078 BioProject: PRJNA895171
Raw data	This paper	https://data.mendeley.com/preview/mnvzj5n25n?a=b1e31a00-88d9-400e-a9c0-da90528d10fc
Experimental models: Cell lines		
HPDE (Ouyang et al.[61])	A gift from Dr. Kelvin K. Tsai, National Health Research Institutes, Taiwan	https://doi.org/10.1016/S0002-9440(10)64800-6
Pan18[62]	A gift from Dr. Chia-Ning Shen, Academia Sinica, Taiwan	https://doi.org/10.1016/j.ebiom.2019.08.044
KPC (Rucki et al.[63])	A gift from Dr. Lei Zheng, Johns Hopkins University School of Medicine	https://doi.org/10.1158/1535-7163.MCT-16-0452
PC080 (Chen et al.[23])	Dr. Wen Hwa Lee's Lab	https://www.ncbi.nlm.nih.gov/pmc/articles/PMC6325483/
PC084 (Chen et al.[23])	Dr. Wen Hwa Lee's Lab	https://www.ncbi.nlm.nih.gov/pmc/articles/PMC6325483/
Mouse primary pancreatic acinar cells	This paper	https://www.ncbi.nlm.nih.gov/pmc/articles/PMC3855917/pdf/jove-78-50514.pdf
3T3-L1	ATCC	CL-173
Experimental models: Organisms/strains		
C57BL/6JNarl mice	Taiwan National Laboratory Animal Center	N/A
NOD/SCIDg mice	The Jackson Laboratory	N/A
Oligonucleotides		
All primers, see Table S1	This paper	N/A
miR-16-5p mimics	Thermo Fisher	Cat# AM17100, PM10339
miR-21-5p mimics	Thermo Fisher	Cat# AM17100, PM10206
miR-29a-3p mimics	Thermo Fisher	Cat# AM17100, PM12499
miR-125b-5p mimics	Thermo Fisher	Cat# AM17100, PM10148
Negative control mimics	Thermo Fisher	Cat# AM17100
Erlin2 siRNA	DharmaFECT	Cat# L-054674-01-0005
CMPK1 siRNA	DharmaFECT	Cat# L-063389-00-0005
MCT1 siRNA	DharmaFECT	Cat# L-058863-01-0005
Negative control siRNA	DharmaFECT	Cat# D-001810-10-05
Recombinant DNA		
pLAS5w-Erlin2-RFP	This paper	N/A
pLAS5w-CMPK1-RFP	This paper	N/A

(*Continued on next page*)

Continued

REAGENT or RESOURCE	SOURCE	IDENTIFIER
pLAS5w-MCT1-RFP	This paper	N/A
SLC16A1-GFPSpark	SinoBiological	Cat# HG16605-ACGLN
pmirGLO-Erlin2-3′UTR	This paper	N/A
pmirGLO-CMPK1-3′UTR	This paper	N/A
pmirGLO-MCT1-3′UTR	This paper	N/A
pmirGLO-Cse1L-3′UTR	This paper	N/A
Myc-His-ATGL	This paper	N/A
Software and algorithms		
Adiposoft	ImageJ-MATLAB	https://doi.org/10.1194/jlr.D023788
GraphPad Prism 9.0	GraphPad Software	https://www.graphpad.com
Gel-Pro Analyzer	Media Cybernetics	https://en.freedownloadmanager.org/Windows-PC/Gel-Pro-Analyzer-FREE.html

RESOURCE AVAILABILITY

Lead contact

Further information and requests for resources and reagents should be directed to the Lead Contact, Chun-Mei Hu (CMHU1220@gate.sinica.edu.tw).

Materials availability

This study did not generate new unique reagents and all materials in this study are commercially available. Plasmids and associated vector maps generated is this study are available upon request. Any additional analysis information for this work is available by request to the lead contact.

Data and code availability

- The mass spectrometry proteomics data have been deposited to the ProteomeXchange Consortium via the PRIDE partner repository with the dataset identifier PXD037862 (http://www.ebi.ac.uk/pride/archive/projects/PXD037862) and PXD037998 (http://www.ebi.ac.uk/pride/archive/projects/PXD037998). Small RNA-seq data that support the findings of this study have been deposited in the Sequence Read Archive (SRA) under the accession codes from SRR22103074 to SRR22103078 within NCBI BioProject PRJNA895171. Raw data has been deposited at Mendeley Data (https://data.mendeley.com/preview/mnvzj5n25n?a=b1e31a00-88d9-400e-a9c0-da90528d10fc).
- This paper does not report original code.
- Any additional information required to reanalyzed the data reported in this paper is available from the lead contact upon request.

EXPERIMENTAL MODEL AND STUDY PARTICIPANT DETAILS

Ethics statement

The pancreatic cancer plasma samples were from the National Taiwan University Hospital, Taipei, Taiwan. Patients were given informed consent and approved by the Institutional Review Board of the NTUH (201612123RIND) and NTUH (201701015RINA).

Human specimens

Plasma samples from Asian subjects were acquired from the National Taiwan University Hospital (NTUH), Taipei, Taiwan. Between 2005 and 2017, peripheral blood of 33 control (Male=15, Female=18, Age: 24-83 years) and 35 pancreatic cancer patients (Male=22, Female=13, Age:40-86 years, Stage I-II: 11, Stage III-IV:24) who underwent pancreaticoduodenectomy in NTUH were collected. Clinical Characteristics of the Patient Sample were shown in Table S2.

Animal protocols, diets, and treatment

The animal experiments were approved by the Institutional Animal Care and Utilization Committee of Academia Sinica, Taipei, Taiwan (IACUC:14-05-709). Male C57BL/6JNarl and NOD/SCIDγ mice at the age of 6-8 weeks were respectively obtained from the National Laboratory Animal Center and The Jackson Laboratory. Mice were maintained in a SPF (specific pathogen-free) animal facility at 20±2°C with a 12/12 hours light/dark cycle and had free access to water and standard laboratory chow diet.

Sample size estimation

We chose our sample sizes based on those commonly used in this field without predetermination by statistical methods. This is stated in the figure legends.

General cell culture and establishment of stable cell lines

Mouse pancreatic cancer cell line (mPDAC) Pan18 cells are kindly gift from Dr. Chia-Ning Shen (Academia Sinica, Taiwan), which were generated from the liver metastatic sites of *Elas-CreER*; *LSL-Kras*$^{G12D/+}$; *Trp53*$^{f/+}$ male mouse treated with cerulean.[62] KPC cells were obtained from Dr. Lei Zheng (Johns Hopkins University School of Medicine) and generated from the primary pancreas site of *Pdx1-Cre*; *LSL-Kras*$^{G12D/+}$; *Trp53*$^{R172H/+}$ male mice.[63] Pan18 cells were cultured with high-glucose-DMEM (Cat: 11965-092, Gibco). KPC cells and human PDAC patient-derived PC080 and PC084 cell lines were cultured in RPMI1640 medium (Cat: 22400-089, Gibco).[23] All the media were supplemented with 10% fetal bovine serum, penicillin and streptomycin (100 IU/ml and 100 μg/ml, respectively), and 1× non-essential amino acids. For exosomes isolation, cells were cultured in Exosomes-depleted FBS-containing medium (Cat: A2720801, Gibco). The non-transformed human pancreatic ductal epithelial cells (HPDE), a gift from Dr. Kelvin K. Tsai, National Health Research Institutes, Taiwan, were grown in keratinocyte serum-free (KSF) medium with 0.2 ng/ml EGF and 30 μg/ml bovine pituitary extract (Invitrogen Life Technologies).[61] The media and supplements were purchased from Gibco (Thermo Fisher Scientific).

To establish the cell line that stably expresses the vector control, Erlin2, CMPK1, or MCT1, 3T3-L1 cells were infected with the lentivirus containing the indicated cDNA and were selected with 2 mg/ml blasticidin.

All cells were cultured at 37°C in a 5% CO2 atmosphere and maintained within 3 months of resuscitation from the frozen aliquots with less than 20 passages for each experiment. The cell lines were authenticated by morphology or by Short Tandem Repeat (STR) analysis by analyzing multiple locations within the genome containing short DNA sequence repeats. The resulting DNA profiles were used to confirm the identity and purity of all cell lines through comparison to the STR reference database in the past 3 years. In addition, all cells were regularly checked for mycoplasma infection and cell morphology to keep cells healthy.

Establishment of syngeneic and xenograft mouse models

Male C57BL/6JNarl mice at the age of 6-8 weeks were obtained from the National Laboratory Animal Center (Taiwan) and orthotopically injected with or without GFP-LUC-tagged mouse PDAC cell lines, Pan18 and KPC. NOD/SCIDγ (NSG) mice at the age of 6-8 weeks (Genomics Research Center, Academic Sinica) were orthotopically injected with GFP-LUC-tagged human PDAC cell lines, PC080 and PC084. 4 weeks after orthotopic implantation, the body composition was measured by Minispec LF50 TD-NMR Body Composition Analyzer based on Time Domain NMR, providing analysis of fat tissue, lean tissue, and free fluid. The experiment was supported by the Taiwan Mouse Clinic, Academia Sinica and Taiwan Animal Consortium. Then, mice were euthanized and the mice, tumors and adipose tissues were weighed for further analysis.

Mouse primary pancreatic acinar cell culture

Primary acinar cells were isolated as described in Gout et al.[64] Briefly, pancreas from 4- to 6-week-old male mice were cut into pieces of 1 mm^3 and enzymatically digested by collagenase IA (Cat: C0130, Sigma-Aldrich) solution for 20-30 min at 37°C. During incubation, pancreas fragments were mechanical dissociated by moving back-and-forth about ten times every five minutes. Acinar clusters were cultured in glucose-free DMEM/F12 (1:1) medium containing 2.5 % FBS, 1 % Penicillin-Streptomycin (PS), 0.25 mg/ml of trypsin inhibitor (Cat:17075-029, Gibco), and 25 ng/ml of recombinant human Epidermal Growth Factor (EGF) (Cat: PHG0311, Thermo Fisher).

METHOD DETAILS

Plasmids and transfections

The lentiviral shRNA expression vectors of pLKO.1-shLacZ, shRab27a (TRCN0000100577), shRab27b (TRCN0000100425) and miRNA sponges (customized) were from the National RNAi Core Facility (Taipei, Taiwan). Mimics of miR-16-5p (cat#AM17100, PM10339), miR-21-5p (cat#AM17100, PM10206), miR-29a-3p (cat#AM17100, PM12499) and miR-125b-5p (cat#AM17100, PM10148) were obtained from Thermo Fisher, Inc. For lentiviral particles production, 293T cells were co-transfected with pCMVΔ8.91, pMD.G and pLKO.1-Rab27 shRNA using TransIT-LT1 (Mirus). For miRNA mimics transfection, 50 nM of miRNA mimics (AM17100, Thermo Fisher) transfection mix was prepared in a Lipofectamine RNAiMax transfection reagent (Thermo Fisher), following the manufacturers protocol and plated on 3T3-L1 cells seeded in 12-well dish. siRNAs for negative control (Cat: D-001810-10-05), Erlin2 (Cat: L-054674-01-0005), CMPK (Cat: L-063389-00-0005) and MCT1(Cat: L-058863-01-0005) were obtained from DharmaFECT (Lafayette, USA).

Protein extraction and western blotting analysis

Cells and tissues were extracted by RIPA buffer [50 mM Tris-HCl, pH 7.4, 150 mM NaCl, 2 mM ethylenediaminetetraacetic acid (EDTA), 0.5% sodium deoxycholate, 0.1% sodium dodecyl sulphate (SDS), 1 mM phenylmethylsulphonyl fluoride (PMSF), 50 mM NaF, 1% Nonidet P-40, protease inhibitor cocktail and phosphatase inhibitor cocktail] and equal protein extracts was loaded and separated in SDS-PAGE followed by transfer to PVDF membranes. After blocking, membranes were incubated with indicated primary antibodies: Anti-Alix (ab186429) and Anti-UCP1(ab10983) were obtained from Abcam, Cambridge, UK. Anti-CD81 (sc-166029) antibody was purchased from Santa Cruz, Dallas, TX,

USA; anti-C/EBPβ (cat:606202) was obtained from BioLegend, San Diego, CA, USA; anti-TSG101 (GTX70255), anti-Erlin2 (GTX106277), anti-CMPK1 (GTX105566), anti-MCT1 (GTX-631643), anti-Cse1L (GTX103005), anti-RFP (GTX127897) and anti-GAPDH (GTX100118) antibodies were from GeneTex, Irvine, CA, USA; anti-Rab27a (Cat:17817-1-AP) and anti-Rab27b (Cat:13412-1-AP) antibodies were obtained from Proteintech, USA; anti-ATGL (2138s) and anti-PPARγ (2443s) antibodies were gained from Cell Signaling Technology, Danvers, MA, USA. Horseradish peroxidase-conjugated goat anti-mouse (111-035-146) and anti-rabbit (111-035-144) secondary antibodies were obtained from Jackson ImmunoResearch. PVDF membrane incubated with primary antibody at 4°C for overnight and then followed by horseradish peroxidase (HRP)-conjugated goat-anti-rabbit or anti-mouse antibody for 1 hr. Signals were detected using Immobilon Forte Western HRP Substrate (Merck Millipore, WBLUF0500) and captured by UVP BioSpectrum 500 Imaging System. The intensity of each band in immunoblotting was quantified using the Gel-Pro software.

RNA extraction and quantitative real-time PCR

Total RNA was extracted from cells, tissues or exosomes using the TRIzol or TRIzol-LS (Life Technologies) as the manufacturer's instructions. The mRNA was reverse-transcribed into cDNA using the Maxima First Strand cDNA Synthesis Kit (Thermo Fisher). For the Exosomal miRNA assay, cDNA was prepared using the miScript II RT Kit (Cat: 218161, QIAGEN, Valencia, CA). To quantify the gene expression, the real-time PCR was performed using SYBR FAST qPCR Kit (KAPA Biosystems, Wilmington, MA, USA) and analyzed on a StepOnePlus Real-Time PCR System (Applied Biosystems, Life Technologies, Carlsbad, CA, USA). GAPDH was used as an internal control for mRNA expression. RNU44 and sno135 were used as the human and mouse miRNAs internal control. Fold changes were calculated by using $2^{-\Delta\Delta Ct}$ method after normalization by internal control. Primer sequences were listed in Table S1.

Histology and quantification of adipose tissues

Adipose tissues were fixed in 4% paraformaldehyde and embedded in paraffin. The sections were counterstained with hematoxylin (Ventana Medical Systems) and scanned by Leica Aperio AT2 Digital Pathology Slide Scanners (Aperio, Leica Microsystems, Vista, CA) at 20 × magnification. The slides were analyzed using ImageJ with the Adiposoft version plug-in. Adipocyte size of white adipose tissues were measured by determining 5 randomly chosen fields (including 1000∼2500 cells/per mice).

Purification of exosomes from conditioned medium

Exosome from conditioned medium s were isolated as described in Thery et al.[26] Briefly, cells were removed from the conditioned media by centrifugation at 400 × g for 10 min. The supernatants were filtered through a 0.22 μm filter, and ultra-centrifuged at 100,000 × *g* for 1.5 hours (Beckman fixed-angle 70 Ti rotor). For further sucrose gradient purification, ultra-centrifuged pellets were resuspended in 20 mM HEPES buffer and gently added above the top of continuous sucrose gradients (bottom to top: 2M, 1.3M, 1.16M, 0.8M, 0.5M and 0.25 M) without disturbing the interface. The gradients were centrifuged for 16 hours at 100,000 × *g*, 4°C, in the SW 41 rotor with the no-brake set, and 0.5 ml fractions were collected from the bottom. Each fraction was measured by O.D. 260 nm and O.D. 280 nm. The fractions of peak (F7 to F10) were collected and washed 3 times with PBS through Amicon Ultra 4 ml centrifugal filters with a cut-off of 100 kD (Millipore, Billerica, MA, USA).

Isolation of exosomes from human plasma and mouse serum

Patient plasma exosomes were purified by Size-exclusion chromatography (SEC). In brief, the plasma from PDAC patients diluted 2 times with PBS were filtered through 0.22 μm filter and centrifuged at 13,000 × *g* for 15 min. The supernatant was loaded on the Sepharose CL-4B column and eluted fractions were collected. Exosomes were concentrated by Amicon Ultra 0.5 ml 30-kDa devices (Millipore, Billicera, MA, USA). Mouse sera were centrifuged at 2,000 x *g* for 30 minutes to remove cells and debris. The clarified serum was added with 0.2 volumes of the Total Exosome Isolation reagent (Cat: 4478360, Thermo Fisher,) and incubated for 30 minutes at 4°C. The mixtures were centrifuged at 10,000 × *g* for 10 minutes at RT. The serum exosomes are enriched in the pellet at the bottom of the tube.

Nanoparticle Tracking Analysis (NTA)

Size distribution and concentration of isolated exosomes were performed using the NanoSight NS300 instrument (Malvern Instruments Ltd, Malvern, UK) equipped with the Nanoparticle Tracking Analysis (NTA) software (versions 3.1 build 3.1.46). The assays were examined as manufacturer's instructions. In brief, the particles of diluted exosomes were injected by syringe pump and recorded for 60 seconds. Three independent video files of the particles moving under Brownian motion were captured and analyzed.

TEM and Cryo-EM

Purified exosomes were resuspended in PBS containing 2% paraformaldehyde and fixed on glow-discharged Formvar/carbon-coated copper grids (Ted Pella, Inc., Redding, CA, USA). The grids were stained with 1% uranyl acetate and imaged by a transmission electron microscope (TEM) (Tecnai G2 F20 X-TWIN, FEI, USA). For cryo-EM, exosomes were flash-frozen in liquid nitrogen within an automated vitrification device (FEI Vitrobot Mark IV, FEI, Hillsboro, OR). The vitrified samples were transferred to a Gatan Cryo holder (Model 626.DH) and visualized in a FEI Tecnai G2 F20 ST TEM (FEI, Hillsboro, OR).

Bio-distribution of exosomes

The 0.22 μm-filtered conditioned medium was incubated with 1 μM fluorescent lipophilic tracer DiR (1,1-dioctadecyl-3,3,3,3-tetramethylindotricarbocyanine iodide) (D12731, Invitrogen, Life Technologies) at room temperature (RT) for 15 minutes and ultra-centrifuged as described above. The DiR-labeled exosomes were administered into mice via the retro-orbital injection and images of individual organs were obtained 24 hours after injection by IVIS 100 imaging system. Living Image software (PerkinElmer, Waltham, MA, USA) was used to analyze the data.

Body composition measurement

Exosomes isolated from cultured medium of acinar cells or pancreatic cancer cells by ultracentrifugation were quantified. Male C57BL/6JNarl mice were received daily injection of 10 μg exosomes for 4 weeks. The body composition was measured by Minispec LF50 TD-NMR Body Composition Analyzer based on Time Domain NMR, providing analysis of fat tissue, lean tissue, and free fluid. The experiment was supported by the Taiwan Mouse Clinic, Academia Sinica and Taiwan Animal Consortium.

Differentiation of pre-adipocyte 3T3-L1

The 3T3-L1 pre-adipocytes were cultured in high-glucose DMEM with 10% calf serum at 37°C in an atmosphere of 5% CO_2. Post-confluent cells were induced by Differentiation medium containing high-glucose DMEM, 10% FBS, 0.25 mM dexamethasone (Sigma D4902), 0.5 mM isobutylmethylxanthine (Cat: I7018, Sigma-Aldrich) and 1 mg/mL of insulin. After 2 days, the cells were maintained in high-glucose DMEM containing 10% FBS and 1 mg/mL of insulin. After another 2 days, medium was changed to high-glucose DMEM containing 10% FBS until the day 8.

Glycerol assay

The glycerol concentration was measured according to the manufacturer's instructions of Glycerol Assay Kit. (MAK-117, Sigma-Aldrich). In brief, 10 μl of appropriate standards or 3T3-L1-cultured medium samples were loaded into 96-well dish and mixed with 100 μl of the Master Reaction Mix to each well. After 20 minutes of incubation, measured the absorbance at 570 nm and calculated the glycerol amount from standard curve.

Oil red staining

Differentiated 3T3-L1 cells were gently washed twice with PBS and fixed with 10% Formalin for 30 minutes. After removing the formalin, the cells were incubated with 60% isopropanol for 5 minutes and stained with Oil Red O (Sigma O0625) to observe the fat droplet formation in 3T3-L1 cells. Fat droplets were extracted by isopropanol and measured in a 96 well plate reader at 492 nm.

Immunoprecipitation

For ATGL immunoprecipitation, cells were lysed in RIPA lysis buffer [50 mM Tris-HCl, pH 7.4, 150 mM NaCl, 2 mM ethylenediaminetetraacetic acid (EDTA), 0.5% sodium deoxycholate, 0.1% sodium dodecyl sulphate (SDS), 1 mM phenylmethylsulphonyl fluoride (PMSF), 50 mM NaF, 1% Nonidet P-40, protease inhibitor cocktail and phosphatase inhibitor cocktail], and the supernatant was incubated with myc-beads at 4°C for 2 hours, or with anti-ATGL antibody or anti-rabbit-IgG antibody at 4°C overnight followed by 1-hour incubation with Protein G beads. Beads were washed three times with RIPA buffer, and proteins were eluted with Laemmli sample buffer and resolved by SDS-PAGE.

ATGL lipase activity assay

Lipase activity was measured as described in Iglesias et al.[65] Briefly, HEK293T cells were transfected with pCDNA3.1-myc-His-ATGL or pLAS5w-RFP-MCT1 and extracted by buffer A (50 mM HEPES, pH 7.2, 100 mM NaCl, 5 mM CaCl2, 0.5 mM DTT, 2% DMSO, 0.1% Triton X-100). The ATGL and MCT1 expression was verified by Western blotting. Using EnzChek lipase substrate (Cat: E33955, Life Technologies) to measure ATGL lipase activity and empty vector-transfected cells were used as control. Assays were performed in 96-well opaque black plates containing 30 μg of cell extract in buffer A. 5 μl of 20 μM EnzChek lipase substrate working solution was added to each well to a final concentration of 1 μM to start the reaction at 37°C. Fluorescence (excitation 485 nm; emission 510 nm) was recorded every 30 s and ATGL activity was calculated by subtracting background activity (no enzyme added). The data were collected after the first 15 min of the reaction with the linear portion of the velocity curve.

Small RNA-seq

For library preparation and sequencing, a total amount of 1 μg Exosomal RNA was used as input material for the small RNA sample preparations. Sequencing libraries were generated using TruSeq Small RNA Library Preparation Kits (Illumina, USA.) following the manufacturer's recommendations. Briefly, 3′ and 5′ adaptors were directly and specifically ligated to 3′ and 5′ end of small RNA, respectively. Then first-strand cDNA was synthesized using SuperScript II Reverse Transcriptase. After PCR amplification, the library was size-selected with 115 – 160 bp on the BluePippin system. The quality of purified libraries was assessed on the Agilent Bioanalyzer 2100 system and a Real-Time PCR system. The qualified libraries were then sequenced on Illumina NextSeq 500 platform with 75 bp single-end reads generated by Genomics, BioSci & Tech Co., New Taipei City, Taiwan.

In-vivo miRNA delivery

miRNA mimics and *in vivo*-jetPEI™ reagent (Polyplus transfection) were respectively diluted in 5 % glucose according to the manufacturer's instructions. The diluted *in vivo*-jetPEI™ was added to the diluted miRNA mimics (900 ng) and incubated for 15 minutes at room temperature. The miRNA complex was one-shot injected into fat pad.

Dual-luciferase reporter assay

3T3-L1 cells were plated in a 24-well plate and co-transfected with a luciferase reporter pmirGLO vector containing the 3'UTR of interest genes (Erlin2, CMPK1, MCT-1 and Cse1L) together with 50 nM of miR-NC, miR-16-5p or miR-29a-3p mimics. Cells were lysed by Passive Lysis Buffer (cat: E1910; Promega Corporation) and agitated at room temperature for 20 min. The luciferase activity was analyzed using a Dual-Glo® Luciferase Assay System (Cat: E2920; Promega Corporation) according to the manufacturer's recommendations. For each transfection, luciferase activity was averaged from three replicates. Luminometry readings were obtained using a luminometer VICTOR3.

LC-MS/MS analysis

Samples were detected by LC-ESI-MS on a Orbitrap Fusion mass spectrometer (Thermo Fisher, San Jose, CA) equipped with with EASY-nLC 1200 system (Thermo Fisher) and EASY-spray source (Thermo Fisher). The digestion solution was injected (5μl) at 1 μl/min flow rate on to easy column (C18, 0.075 mm X 150 mm, ID 3 μm; Thermo Fisher) Chromatographic separation was using 0.1% formic acid in water as mobile phase A and 0.1% formic acid in 80% acetonitrile as mobile phase B operated at 300 nl/min flow rate. Briefly, the gradient employed was 2% buffer B at 2min to 40% buffer B at 40 min. Full-scan MS condition: mass range m/z 375-1800 (AGC target 5E5) with lock mass, resolution 60,000 at m/z 200, and maximum injection time of 50 ms. The MSMS was run in top speed mode with 3s cycles with CID for protein id or ETD for phosphopeptide; while the dynamic exclusion duration was set to 60 s with a 10 ppm tolerance around the selected precursor and its isotopes. Electrospray voltage was maintained at 1.8 kV and capillary temperature was set at 275°C. Raw file processed by Maxquant (Version 1.6.15). MSMS spectra was search against the uniprot yeast database (6049 entries) and enzyme digest by trypsin with 2 miss cleavage. The parameter such as MS tolerance of 20ppm for first search and main search 6 ppm. Fragment tolerance was 0.5Da (IT) or 0.01 Da (FT). Variable modification of oxidation (M) and acetylation (protein N-terminal) and fixed modification of carbamidomethyl(C) as search parameters. The mass spectrometry proteomics data have been deposited to the ProteomeXchange Consortium via the PRIDE partner repository with the dataset identifier PXD037862 and PXD037998.

In situ proximity ligation assay (PLA)

This assay was performed using the *Duolink® In Situ* Fluorescent Detection Reagents (Sigma, DUO92008) as the manufacturer's instructions. In brief, 3T3-L1 cells were fixed by 4% paraformaldehyde and permeabilized by 0.5% Triton-X100 for 5 min at RT. The slides were further blocked and incubated with primary antibodies (ATGL and MCT1 antibody,1:100) at 4°C for overnight. The slides were washed and incubated with PLA anti-Rabbit PLUS probe (Sigma, DUO92002) and PLA anti-mouse MINUS probe (Sigma, DUO92004) for 1 hour at 37°C. The ligation and amplification steps were respectively performed in a pre-heated humidity chamber for 30 mins and 100 mins at 37°C. Afterwards, the slides were mounted with *Duolink® In Situ* mounting media (with DAPI), following analyzed by SP5 Confocal microscope (Leica Microsystems).

QUANTIFICATION AND STATISTICAL ANALYSIS

Statistical analysis

Data were presented as means ± SD as indicated in figure legends. Student's t-test and Pearson's correlation coefficient were used for testing the difference and correlation between control and experimental groups. * Indicated statistical significance with $p < 0.05$, ** indicated statistical significance with $p < 0.01$, and *** indicated statistical significance with $p < 0.001$. N number used in indicated section was shown in the figure legends.